Interhelical interactions between D92 and C218 in the cytoplasmic domain regulate proton uptake upon N-decay in the proton transport of *Acetabularia* rhodopsin II

Jun Tamogami[1,*], Takashi Kikukawa[2,3], Keisuke Ohkawa[1], Noboru Ohsawa[4,5], Toshifumi Nara[1], Makoto Demura[2,3], Seiji Miyauchi[1,7], Tomomi Kimura-Someya[4,5], Mikako Shirouzu[4,5], Shigeyuki Yokoyama[4,6], Kazumi Shimono[1,7,#] and Naoki Kamo[1,2]

[1]College of Pharmaceutical Sciences, Matsuyama University, Matsuyama, Ehime 790-8578, Japan

[2]Faculty of Advanced Life Science, Hokkaido University, Sapporo 060-0810, Japan

[3]Global Station for Soft Matter, Global Institution for Collaborative Research and Education, Hokkaido University, Sapporo 001-0021, Japan

[4]RIKEN Systems and Structural Biology Center, Yokohama 230-0045, Japan

[5]RIKEN Center for Life Science Technologies, Yokohama 230-0045, Japan

[6]RIKEN Structural Biology Laboratory, Yokohama 230-0045, Japan

[7]Graduate School of Pharmaceutical Sciences, Toho University, Funabashi, Chiba 274-8510, Japan

*Correspondence: jtamoga@g.matsuyama-u.ac.jp

[#]Present address: Faculty of Pharmaceutical Sciences, Sojo University, Kumamoto 860-0082, Japan

Running title: Interhelical interaction between D92 and C218 in *Acetabularia*

rhodopsin II

Keywords: microbial rhodopsin, proton pump, photocycle, hydrogen bond, switching

Abbreviations

AR, *Acetabularia* rhodopsin; BR, bacteriorhodopsin; ChR2, channelrhodopsin-2; PR, proteorhodopsin; ATR, all-*trans* retinal; PSB, protonated Schiff base; SB, deprotonated Schiff base; CP, cytoplasmic; EC, extracellular; H-bond, hydrogen bond; λ_{max}, absorbance maximum wavelength; P_i, *i*th photochemically-defined state determined by global fitting; DDM, n-dodecyl-β-D-maltoside; PC, L-α-phosphatidylcholine; ITO, indium-tin oxide; MES, MOPS, HEPES, CHES, CAPS, all abbreviations of Good's buffers

Abstract

Acetabularia rhodopsin II (ARII or Ace2), an outward light-driven algal proton pump found in the giant unicellular marine alga *Acetabularia acetabulum*, has a unique property in the cytoplasmic (CP) side of its channel. The X-ray crystal structure of ARII in a dark state suggested the formation of an interhelical hydrogen bond between $C218^{ARII}$ and $D92^{ARII}$, an internal proton donor to the Schiff base (Wada *et al.*, 2011). In this report, we investigated the photocycles of two mutants at position $C218^{ARII}$: $C218A^{ARII}$ which disrupts the interaction with $D92^{ARII}$, and $C218S^{ARII}$ which potentially forms a stronger hydrogen bond. Both mutants exhibited slower photocycles compared to the wild-type pump. Together with several kinetic changes of the photoproducts in the first half of the photocycle, these replacements led to specific retardation of the N-to-O transition in the second half of the photocycle. In addition, measurements of the flash-induced proton uptake and release using a pH-sensitive indium-tin oxide electrode revealed a concomitant delay in the proton uptake. These observations strongly suggest the importance of a native weak hydrogen bond between $C218^{ARII}$ and $D92^{ARII}$ for proper proton translocation in the CP channel during N-decay. A putative role for the $D92^{ARII}$-$C218^{ARII}$ interhelical hydrogen bond in the function of ARII is discussed.

1. Introduction

Microbial rhodopsins are a family of photoreceptive membrane proteins broadly distributed in various microorganisms, such as archaea, eubacteria, and lower eukaryotes [1-4]. Notwithstanding their diverse functions, microbial rhodopsins possess common properties, which are often described as structural and photochemical similarities. These proteins are commonly composed of seven transmembrane α-helical bundles (helices A-G) and enclose an all-*trans* retinal (ATR) as a chromophore. ATR covalently attaches to a conserved lysine residue on helix G of the opsin, which forms a protonated Schiff base (PSB) linkage [5]. Thus, these proteins can be photoactivated by the absorption of visible light. Light irradiation induces the isomerization of the retinal from all-*trans* to 13-*cis*, initiating a stepwise cyclic photochemical reaction via several photointermediates called the photocycle. During the photocycle, microbial rhodopsins perform their respective functions, including ion pumping, channeling, and photosensing [3,6].

Among many microbial rhodopsins, bacteriorhodopsin (BR), which acts as a light-driven outward proton pump, is the most well-studied [7-10]. The proton transport of BR is essentially accomplished via three main groups associated with proton transfer events: a protonated/deprotonated Schiff base (PSB/SB), its proton acceptor $D85^{BR}$, and donor $D96^{BR}$, which are located at the center of the protein, the extracellular (EC), and the cytoplasmic (CP) transmembrane region of helix C, respectively. In addition, two groups on the EC and CP side modulate the unidirectional proton movement in BR. A proton-releasing complex, which is established by several amino-acid residues and water molecules in the EC channel, causes the ejection of a proton towards the external bulk medium during the first half of the photocycle and subsequently receives a proton

from $D85^{BR}$ during the second half of the photocycle. Another crucial residue is $T46^{BR}$ on helix B, the side chain of which forms a hydrogen bond with protonated $D96^{BR}$ in the CP domain in the unphotolyzed state. This interhelical interaction contributes to the maintenance of the high pK_a of $D96^{BR}$ (> ~11 [11]) at the initial state together with the hydrophobic residues surrounding it [12]. Through the entry of water via the outward tilt of helix F into the CP region at the site of the photoproduct, $D96^{BR}$ forms a new interaction with nearby water chains concurrently with the disruption of the H-bond with $T46^{BR}$ [13]. This H-bonding rearrangement leads to the lowering of the pK_a in $D96^{BR}$ from greater than 11 to approximately 7 [14,15], with subsequent proton donation of $D96^{BR}$ to SB. $T46^{BR}$, via this interhelical interaction, thereby regulates the function of $D96^{BR}$ in the CP region and facilitates efficient proton translocation in BR, although this residue itself does not directly participate in the proton transfer events.

Acetabularia rhodopsin (AR) is a light-driven proton pump found in a marine alga, *Acetabularia acetabulum*, whose characterization was first performed by Hegemann and colleagues [16]. Two AR homologue genes differing from the initially identified AR were subsequently cloned by Jung and colleagues: *Acetabularia* rhodopsin I and II (ARI and ARII, also abbreviated as Ace1 and Ace2, respectively) [17,18]. Previous electrophysiological studies revealed that these two AR proteins function as an outward proton pump, like BR [17,18]. However, their detailed characterization has not progressed due to their relatively low expression in a general host, such as *E. coli*, in the absence of certain modifications [19]. Recently, a unique cell-free protein expression method developed by Shimono *et al.* [20] enabled the large-scale synthesis of the two ARs, allowing accelerated investigation of their photochemical and structural properties [18,21,22].

We previously determined the X-ray crystal structures of ARI and ARII [18,21]. In both, the residues corresponding to $T46^{BR}$ were substituted by asparagine ($N48^{ARI}$ and $N45^{ARII}$, respectively). The oxygen and nitrogen atoms on the side chains of these asparagine residues interact with two carboxyl oxygens of putative proton donor residues ($D100^{ARI}$ or $D92^{ARII}$) through two H-bonds (see Fig. 1B and ref. [21]). Although the role of $N48^{ARI}$ or $N45^{ARII}$ has not been yet clarified, these interactions might provide stabilization of the protonation state of proton donors in the resting state, instead of the T46-D96 interaction in BR. In addition, a unique feature was found in the CP region of ARII. In the structure of the unphotolyzed ARII, at 3.2-Å resolution [18], $C218^{ARII}$ on helix G was located in the neighborhood of $D92^{ARII}$ on helix C (Fig. 1B), although the distance (approximately 3.9 Å) is somewhat far compared to the typical H-bond cutoff distance of 3.2 Å [23]. The residue corresponding to $C218^{ARII}$ is usually a hydrophobic one in many microbial rhodopsins, thus, this is specific for ARII. If $C218^{ARII}$ directly interacts with $D92^{ARII}$ in the dark state, it is likely that a sulfhydryl group of $C218^{ARII}$ forms a weak H-bond with a carbonyl oxygen ($O_{\delta 2}$) on the side chain of protonated $D92^{ARII}$, which serves as a H-bond donor (Fig. 1C). From FTIR spectroscopic studies by Nack *et al.*, a similar Asp-Cys interaction was identified in channelrhodopsin-2 (ChR2), a light-gated cation channel [24]. They proposed that this interhelical interaction on helices C and D acted as a molecular switch (called the DC gate) to control the lifetime of the conductive state in ChR2 [24]. However, the existence of a functional Asp-Cys interhelical interaction in the proton-pumping rhodopsins has not been yet reported. Since it is unclear whether the Asp-Cys interaction implied by the crystal structure of ARII in the dark state is formed even in the photolyzed state and functional, we herein investigated the effects of replacement of

$C218^{ARII}$ on the photoreactivity of ARII. The present study is the first report in which the effects of the Asp-Cys interaction on the photochemistry of a proton-pumping rhodopsin are described, and provides implications for its functional role.

2. Materials and methods

2.1.Sample preparation

Plasmids for the expression of $D92N^{ARII}$ and two $C218^{ARII}$ mutants ($C218A^{ARII}$ and $C218S^{ARII}$) were prepared by PCR using the QuikChange site-directed mutagenesis kit (Stratagene). In this mutagenesis procedure, a previously constructed expression plasmid for the cell-free protein synthesis of the wild-type ARII [22] was employed as a template. The sequences of the PCR product were confirmed using an automated DNA sequencer (Applied Biosystems). The expression and purification of ARII mutant proteins were performed as described previously [18].

2.2.Flash photolysis

Flash photolysis experiments were conducted using the same apparatus and procedure as previously described [25]. A laser pulse (Nd:YAG 532 nm, 7 ns, 5 mJ/pulse) was employed as a pump light. The temperature was maintained at 20°C with a thermostat (NCB-1200; Eyela). The solution for measurements contained 400 mM NaCl, 0.05% n-dodecyl-β-D-maltoside (DDM), and 6 mixed buffers (citrate, MES, HEPES, MOPS, CHES, CAPS, at 10 mM each). The medium pH was adjusted to be desired values by the addition of diluted HCl or NaOH solutions. The concentration of ARII mutant proteins in the sample solution was ~4-5 μM.

Global fitting analysis, assuming an irreversible sequential scheme including

quasi-equilibria [26], was performed for the obtained data by flash photolysis at pH 7.0. The details of this analysis were described in several previous publications [27-29]. Briefly, through simultaneous fitting using a multiexponential function for the dataset at wavelengths from 340 to 700 nm with a 10-nm interval, the optimal number of exponents in the fitting function was determined from the reductions in the standard deviations of the weighted residuals. From this analysis, the time constant (τ_i) of the P_i-state, which represents the *i*th-appearing photochemically-defined state in the determined scheme, and the absorbance difference ($\Delta\varepsilon_i$) between P_i and P_0 (the dark state) were calculated. Regression analysis of the data was performed using Microcal Origin software (Microcal Software) and Igor Pro software (WaveMetrics).

The flash photolysis data at the pH values other than 7.0 were collected at three characteristic wavelengths for ARII, 400, 520, and 610 nm, which primarily monitor the M-state, resting state, and red-shifted K- and O-states, respectively.

2.3.Measurement of absorption spectra at the dark state and determination of photointermediate spectra during the photocycle

The absorbance spectra in the dark state were measured using a spectrophotometer (V-560; Jasco). The obtained spectra contained the effects of the background scattering. Thus, this effect, which is represented as $A+B/\lambda^4$ (λ in nanometers), was removed from each spectrum. To calculate the spectra of the P_i-states determined by the global fitting analysis, the scattering-removed spectra in the dark (P_0) were added to $\Delta\varepsilon_i$.

To estimate the absorbance spectra of the photoproducts, the obtained P_i-spectra were further analyzed using the following equation, represented by the sum of the skewed Gaussian functions [26,30]:

$$\mathrm{Abs}(\lambda) = \sum_{i=1}^{k} A_{i,\max} \cdot \exp\left\{ -\frac{\ln 2}{(\ln \rho_i)^2} \left[\ln\left(\frac{10^7 \left(1/\lambda - 1/\lambda_{i,\max}\right)\left(\rho_i^{\,2} - 1\right)}{\Delta\nu_i \cdot \rho_i} + 1 \right) \right]^2 \right\} \quad (k=2 \text{ or } 3),$$

where Abs (λ) is the absorbance, $\lambda_{i,\max}$ (in nanometers) is the absorbance maximum of the *i*th absorption band, $A_{i,\max}$ is the amplitude at $\lambda_{i,\max}$, ρ_i is the parameter of skewness in the *i*th absorption band, and $\Delta\nu_i$ is the half-bandwidth of the *i*th absorption band (in reciprocal centimeters). The fitting of the data was performed using Igor Pro software (WaveMetrics).

2.4.Measurement of the photoinduced proton release and uptake

Experiments were performed using the same apparatus and procedure as described previously [22,31]. Distilled water suspensions of 100 μL volumes containing ARII mutant proteins (conc. ~1-3 μM), which were reconstituted into 100-fold levels of L-α-phosphatidylcholine (PC) from egg yolks (Avanti) at a molar ratio, were attached to the surface of an indium-tin oxide (ITO) transparent electrode (Techno Print Co.) under reduced pressure. A 300 W Xenon lamp with a cold-mirror was used as the light source for excitation of the proteins. When the light was used to irradiate the proteins for 2 ms through an IR filter (HA50; Toshiba) and a cut-off optical filter (Y44; Toshiba), the evoked photoinduced voltage changes were measured through an AC amplifier (MEG-1200; Nihon Kohden) with a low-cutoff electric filter, whose frequency was set to a high-pass 0.08 Hz. Medium containing 400 mM NaCl and 6 mixed buffers (citrate, MES, HEPES, MOPS, CHES, CAPS, at 1 mM each) was used for measurements. All

experiments were conducted at room temperature (~25°C).

3. Results

3.1. The importance of C218^{ARII} as a preferable hydrogen bonding partner of D92^{ARII} for modulation of overall photocycle kinetics

We first evaluated whether D92^{ARII} (corresponding to D96^{BR}) acts as a proton donor for SB. As anticipated, the neutralization of D92^{ARII} (D92N^{ARII}) caused a remarkable slowing of the M decay, similar to D96N^{BR} (Fig. S1A).

Next, we introduced two types of mutations into C218^{ARII} to examine its role in the photocycle and accompanying proton transfer. One mutation was a C-to-A replacement to disrupt the interaction between D92^{ARII} and C218^{ARII}, if it exists. In another mutant, C218^{ARII} was replaced by serine, which has a hydroxyl group as a side chain and is a potential amino acid residue that forms a H-bond with D92^{ARII}. Figure 2 shows flash-induced absorption changes at three wavelengths (400, 530, and 610 nm) in the wild-type and the two mutants at neutral pH (~7). From global fitting analysis for the dataset at varying wavelengths, including these three traces, a sufficiently fit model for the wild-type was previously determined as a scheme containing five kinetically defined P-states [22]. However, the same analysis for C218A^{ARII} and C218S^{ARII} revealed that the best fit functions for their photocycles were composed of the sum of only four exponential terms.

As shown in Fig. 2, the completion of the photocycles in both C218^{ARII} mutants was slower than that of the wild-type. The time constants of the rate-limiting reaction (P_4-decay) in the photocycle of the two C218^{ARII} mutants were 51.8 ms for C218A^{ARII} and 261.7 ms for C218S^{ARII} (Table 1), which are approximately 2.5- and 12.5-fold

slower than in the corresponding process of the wild-type (P_5-decay, τ_5 ~20.9 ms), respectively. Unexpectedly, the turnover rate of C218S^{ARII} was approximately five-fold slower than that of C218A^{ARII}. The difference of the kinetics between two mutants may be considered that the replacement of C218^{ARII} by serine did not disrupt the H-bond, but rather caused the formation of the distinct interaction from in the wild-type. Considering the higher polarity of the O-H group on the side chain of the serine compared with that of the S-H group of the cysteine, a more robust H-bond may be formed between D92^{ARII} and the introduced residue (S218^{ARII}) compared to the native one in the wild-type. Therefore, the stronger Asp-Ser interaction, at least at the dark state, may be disadvantageous for the more efficient proton-pumping photocycle of ARII, suggesting the preferability of cysteine as a weak H-bonding counterpart of D92^{ARII} rather than serine.

3.2.Effects of replacement of C218^{ARII} on the rise and decay of the photoproducts revealed by spectral decomposition of the kinetic photocycle intermediates (P_i-states)

A series of characteristic photoproducts for proton-pumping rhodopsins, such as K, L, M, N, and O, which are linked by reversible equilibrium reactions, appear during the photocycle of ARII [22]. Therefore, P_i (i=1-5 (wild-type) or -4 (mutants)) spectra obtained through global fitting analysis contain a quasi-equilibrated mixture of several photointermediates. To estimate the contributions of each photoproduct in P_i spectra at neutral pH, these spectra were separated into putative absorption bands of each species using skewed Gaussian functions (see the Materials and Methods section). The results of the spectral decomposition are shown in Fig. 3. The determined spectral parameters

for respective photointermediates, including their λ_{max} values, are listed in Table S1.

As shown in panel (a) of Fig. 3, P_1 spectra in three ARII proteins contained a weaker absorption band at the wavelength region near 400 nm, as well as a red-shifted band. The former band presumably originated from the β-band [32], although three peaks of its fine structure were not clearly observed due to their small absorbance. The peak position of the latter band was different among the three proteins. The λ_{max} of the red-shifted bands in the wild-type and C218S^{ARII} was approximately 560 nm, whereas that of C218A^{ARII} was located at a shorter wavelength (~540 nm). In addition, this band in C218A^{ARII} was somewhat wide. Therefore, we speculated that P_1-states in the wild-type and C218S^{ARII} represent only a red-shifted early photoproduct K, while that in C218A^{ARII} is a mixture of two states, K and most-likely L.

P_2 spectra possess two absorption bands (panel (b) in Fig. 3). Of these two bands, one is an absorbance band with a λ_{max} at a shorter wavelength (~394 nm). Generally, this band, whose spectral property was nearly identical among the three proteins, was due to the M-state. The peak values of other absorption bands in C218A^{ARII} and C218S^{ARII} were blue-shifted compared to that of the wild-type. We tentatively assigned the band of the wild-type to L in our previous publication [22]. However, in the present article, we conclude that this band should be reassigned to K because its λ_{max} (~560 nm) is rather close to the red-shifted band observed in P_1. Note that rigorous inspection reveals that the observed values slightly deviate from the calculated K + M spectrum because of the existence of a small plateau absorption band located at approximately 450-550 nm (Fig. 3Ab), which may imply the presence of a small fraction of L. Therefore, we inferred that L in the wild-type is difficult to accumulate, probably due to its fast decay or rapid reverse reaction to K.

In contrast, P_2-states in C218A^{ARII} and C218S^{ARII} have no K (Figs. 3Bb and 3Cb). Instead, P_2 contains a band with a peak at a shorter wavelength (~510-520 nm) than that of K. In general, this band may be assignable to L. Thus, the replacement of C218^{ARII} may lead to faster K-decay or not prominent L → K reverse reactions. The earliest kinetic photoproduct (P_1) in the D92N^{ARII} mutant also appeared to contain a large amount of L (Fig. S1B). Thus, the results of these mutational experiments suggest that interhelical H-bonding changes due to the replacement of either D92^{ARII} or C218^{ARII} affect the kinetics of K-L and/or L-M transitions.

In addition to the bands of M, P_3 and P_4 spectra had another red-shifted bands, and their bandwidth appeared to be somewhat broadened compared with the red-shifted K-bands in P_1 and P_2 (panels (c) and (d) in Fig. 3A). As reported previously [22], a long M-N-O equilibrium is created during the latter half of the photocycle in ARII. Therefore, these red-shifted bands may represent a mixture of N and O. Forward or reverse reactions may predominate, depending on the pH, in the equilibrium between M and N or N and O. Under acidic conditions (pH ≤ ~5.5), N was not accumulated because of the facilitated N → O forward reaction. Instead, two O-states (O_1 and O_2) were produced [33]. The former O (O_1) may not be observable at neutral pH for kinetic reasons. Thus, the latter O (O_2) may correspond to the O-intermediate observed at neutral and basic pH values. We estimated a pure spectrum of O (O_2) from the analysis using skewed Gaussian functions for the P_4-spectrum at pH 5.0 (Fig. S2A). The absolute spectrum of N was estimated from the same analysis for P_4 at pH 8.6, where N and O coexist but the fraction of N is predominant compared to O due to its slow decay (Fig. S2B). Using the calculated spectral parameters for N and O, except for their amplitudes (A_{max}), the red-shifted bands in P_3 and P_4-states were analyzed.

In P_3 of the wild-type, the fraction of M was the largest among the three photoproduct states, which may be attributed to the rapid reverse reaction from N to M. Since M and O are in a quasi-equilibrium state via N, the first and second phases in the biphasic decay of the absorbance change at 400 nm (ΔA_{400}), which may reflect the processes of the M(N)O-quasi-equilibrated state's formation from M and its decay, respectively (Fig. 2A). Therefore, the more rapid M → N forward reaction led to the relatively larger amplitude of the first decay phase and the smaller amplitude of the second decay phase in the overall decay phase of ΔA_{400}. Conversely, the faster N → M reverse reaction led to the opposite result. Therefore, the larger amplitude of the second slower phase compared to that of the faster one in the decay of ΔA_{400} of Fig. 2A signifies a faster N-to-M reverse reaction compared with the forward reaction, which is consistent with the observation of the large fraction of M in the MNO-quasi-equilibrated P_3-state (Fig. 3Ac).

The fraction of N (λ_{max} ~526 nm) in P_3 was significantly smaller than that of O (λ_{max} ~562 nm) (Fig. 3Ac). This may be associated with a relatively faster N-decay at this pH in addition to the facilitated N-to-M reverse reaction described above. The red-shifted band in P_4 can be almost approximated as a spectral band of a single O (Fig. 3Ad), suggesting slight N-accumulation during the photocycle at neutral pH.

In contrast to the wild-type protein, P_3 and P_4 of the two $C218^{ARII}$ mutants included a relatively small fraction of M (panels (c) and (d) in Figs. 3B and C). The fractions of M and N in P_3 of $C218A^{ARII}$ were almost comparable (Fig. 3Bc), whereas the fraction of N in P_3 of $C218S^{ARII}$ was much larger than that of M (Fig. 3Cc). These results are approximately consistent with the ratios of the amplitude of faster and slower decay components of the ΔA_{400} signals in Figs. 2B and C. Thus, the N → M reverse reaction in

these mutants was not as pronounced, unlike in the wild-type. Moreover, the fraction of N was much larger than that of O. With the transition from P_3 to P_4, the fraction of O in the wild-type slightly increased (Fig. 3Ac and d). In contrast, the fraction of N in the P_4-states of C218A^{ARII} and C218S^{ARII} remained predominant (Figs. 3Bd and 3Cd), implying a shift of the equilibrium between N and O towards N, i.e., a slower N-decay in mutants.

P_5 in the wild-type had an absorbance band with a λ_{max} (~532 nm) close to that of the dark state (Fig. 3Ae), assigned to ARII' previously [22]. In contrast, a P_5-state was not observed in C218A^{ARII} and C218S^{ARII}. The lack of detectable ARII' in these mutants may be involved in the prolonged N-decay during their photocycles.

3.3.Differences in the photocycles of the two C218^{ARII} mutants from the wild-type at various pH values

To further investigate the impact of the replacement at C218^{ARII} on the photocycle, flash photolysis experiments for C218A^{ARII} and C218S^{ARII} were performed at varying pH values (Fig. S3). The representative results for two C218^{ARII} mutants at four characteristic pH values are shown in Fig. 4. Different features in the photocycles of the mutants from that of the wild-type (shown as dotted, broken, and chain lines) included: 1) a faster K-decay (M-rise) in both mutants, which was observed particularly clearly at low pH values, 2) a slower O-decay under acidic conditions, 3) no observation of O at substantially lower pH than in the wild-type (7.5 (mutants) vs 8.8 (wild-type [22])) as an increase in pH, and 4) the formation of a M_a-like photoproduct (shown by the bold arrow in Fig. 4Bd) in the photocycle of C218S^{ARII} at alkaline pH values (8.5 and 9.0), as observed for proteorhodopsin (PR) from marine bacteria [34]. These points are

described in the Supplementary materials (see the captions of Figs. S4 and S5). In addition to the findings described above, the photocycle rates of two mutants are appreciably slower than those of the wild-type in all pH ranges. Although the reason for the slowing of O-decay at acidic pH values (2) is unknown, changes in the interaction of $D92^{ARII}$ on helix C with $C218^{ARII}$ on helix G by these mutations may influence the deprotonation of the PSB counterion $D81^{ARII}$, on the same helix C as $D92^{ARII}$, during the O-decay. Moreover, the appearance of unusual branch reactions with the formation of M_a in $C218S^{ARII}$ (4) may suggest that the H-bonding partner of $D92^{ARII}$ should be cysteine. Note that the similar photocycle branch in PR reduced the outward proton-pumping current [34].

3.4.pH dependence of multiple decay components of absorption changes at 400 nm

The decay of ΔA_{400} changes from mono- to bi- or triphasic with an increase in pH (Figs. 4 or S3). This tendency is similar to that of the wild-type [22]. As described previously [22], the appearance of this pH-dependent multiexponential decay is relevant for the formation of the equilibrium between M, N, and O with increasing pH. Because of the existence of this equilibrium between three photoproducts, it is difficult to separately estimate the rise/decay rates of respective states and examine the pH dependence of the kinetics of each. Thus, we attempted to investigate the pH dependence of these photoproducts from an analysis of the ΔA_{400} signals because the decay of ΔA_{400}, which mainly reflects M-decay, is also influenced by the kinetics of the other photoproducts N and O. The upper panels (a) in Fig. 5 show close-ups of the ΔA_{400} for $C218A^{ARII}$ and $C218S^{ARII}$ at three characteristic pH values. The decaying phases of these signals were analyzed using the following equation with single, double, or triple

exponential terms:

$$\Delta A_{400} = \sum_{i=1}^{n} A_i \exp\left(-t/\tau_i\right) \quad (n=1 \text{ or } 2 \text{ or } 3)$$

where A_i and τ_i signify the amplitudes and time constants of the ith decay components. The decay time constants at respective pH values were estimated from the fitting noted above.

The lower panels (b) in Fig. 5 show the plots of three decay time constants in C218A^{ARII} and C218S^{ARII} as a function of pH. The inset of Fig. 5Ab represents the corresponding plot of the wild-type. As seen similarly in these plots, τ_1 and τ_2 are almost independent of pH, although τ_1 appears to slightly decrease with acidification of the medium pH below approximately 6. Conversely, τ_3 apparently shows pH-dependence. From a comparison with the lifetime values of P_i-states at pH 7.0 (Table 1), τ_1, τ_2, and τ_3 in C218A^{ARII} and C218S^{ARII} are approximately consistent with the time constant values of P_2, P_3, and P_4-decay, respectively. As seen in Fig. 3B and C, the P_2-to-P_3 conversion in C218A^{ARII} and C218S^{ARII} accompanies the transition from M (+L) to the quasi-equilibrated mixture of M, N, and O. Judging from a little bit of O in the P_3-states (Fig. 3Bc and 3Cc), τ_1 in C218^{ARII} mutants may primarily reflect the formation of the M, N-quasi-equilibrium state from M. During the M-to-N transition, the internal proton transfer from D92^{ARII} to SB most likely occurs, which may account for the nearly pH-independent behavior of the τ_1-plots. Along with the P_3-to-P_4 transition with the time constant of τ_2, the fraction of N further increases at the expense of M. In the formed MNO-quasi-equilibrated P_4-state after this transition, N was most dominant. Therefore, the major determinant in the recovery of the original state from

the P_4-state (τ_3) may be N-decay. Thus, the pH-dependence of τ_3 implies that N-decay is accompanied by proton transfer from the external media. In the corresponding graphs of the wild-type, both of the third decaying phases of ΔA_{400} at near neutral pH (~7) (the inset of Fig. 5Ab) and the large fraction of N in the P_3 and P_4-states (Fig. 3Ac and d) were not observed because of the relatively faster N-decay at this pH value. However, an increase of the pH above 7.3 gave rise to the appearance of τ_3, with the large accumulation of N in P_4 (lower panel (b) of Fig. S2B). It is noted that the pH-dependency of τ_3 in the wild-type can be interpreted in the same way as in the case of $C218A^{ARII}$ and $C218S^{ARII}$, although N does not appear obviously in P_4 of the wild-type at pH $\leq$ ~7.

Comparison of the τ-plots between the wild-type and $C218^{ARII}$ mutants revealed an important finding that in contrast to the similarity of the pH dependence of τ_1 and τ_2 among all proteins, there was the difference in the N-decay kinetics, which could be roughly estimated from τ_3 values. The plots of τ_3 in three ARII proteins showed a linear pH-dependence with almost similar slopes (approximately 0.55 for the wild-type, approximately 0.60 for $C218A^{ARII}$, and approximately 0.64 for $C218S^{ARII}$). The slopes of these plots were less unity. The reason for this shared slope reduction is unclear at present, but a possible explanation may be the difference in the pH between the protein surface and the bulk due to negative charges of proteins [35]. In contrast, the plotted absolute values of τ_3 of $C218^{ARII}$ mutants were markedly different from those of the wild-type (shown as the broken line). The approximately 10-30-fold larger τ_3 values of $C218^{ARII}$ mutants demonstrate a substantial delay of N-decay in these mutants. This is consistent with the conclusion drawn from the results of the spectral analysis of kinetic P_3 and P_4 states (panels (c) and (d) in Fig. 3).

3.5.Direct observation of delayed proton uptake with replacement of C218^{ARII}

As described above, the observation of the pH dependence of τ_3 implies that the proton uptake from the media occurs upon N-decay and is delayed by the replacement of C218^{ARII}. To further obtain evidence for this slowing of proton uptake, we measured the proton uptake/release in the C218^{ARII} mutants during their respective photocycles and compared with that of the wild-type. Measurements at near neutral pH values led to the small magnitude of proton transfer signals with the initial proton uptake followed by release. This small signal is probably because of cancellation of opposite two proton transfer sequences which are composed of the first proton uptake followed by release and the reverse sequence [22]. With increasing pH above 7.5, the signal with the first proton release followed by uptake became predominant in the mixture of two signal sequences, resulting in that the sufficient large magnitude of signal was observed because of the lack of the cancellation [22]. Thus, we performed experiments at pH above neutral. Instead of the conventional method using pH-indicator dyes, we adopted an experimental technique using an ITO transparent electrode because this method more sensitively responses to the change of the external pH with the photoinduced proton uptake/release and can be applied to measurements over the wide pH range including alkali conditions. In addition, we previously confirmed that this experimental system can work as a time-resolved pH electrode at the millisecond timescale [31]. Note that experiments were conducted in samples reconstituted into lipids (egg-PC), while flash-photolysis measurements were done in detergent. Thus, when the data of two different experiments are compared, we should pay attention to the effects by different sample preparations, e.g., a difference in their time courses. Figure 6 shows

flash-induced ITO signals in C218A^{ARII} and C218S^{ARII} mutants at pH 8.5. In this figure, the proton release and uptake during the photocycle are represented by the upward and downward deflections, respectively. We found that the first proton release that probably occurs from E199^{ARII} (corresponding to E204^{BR}) is followed by uptake under this pH condition, in agreement with the order of proton transfer in the wild-type at the same pH value (gray solid lines) (also see ref. [22]). Comparison of time courses of the decreasing phases representing proton uptake in C218A^{ARII} and C218S^{ARII} with that of the wild-type revealed that the proton uptake in these mutants markedly slows down (also see time constants of the latter H^+-uptake in each protein in Fig. S6). Thus, these observations are supportive of the delay of N-decay in parallel with proton uptake with the replacement of C218^{ARII}.

4. Discussion

In this study, we evaluated the influence of two types of substitutions at C218^{ARII}, C-to-A or -S mutations, on the photocycle and accompanying proton transfer. These replacements gave rise to several minor alterations in the first half of the photocycle. In addition to the observation of faster K-decay at acidic pH (Fig. 4), the apparent detection of the fraction of L in P_2-spectrum at neutral pH (Fig. 3) indicates that the kinetics change of K-to-L and/or L-to-M transition with the mutations. It was reported that the transition from K to L in BR is accompanied by important structural changes in the CP domain, such as reorientation of the N-H bond of PSB towards the CP side, upward movement of the C13 methyl group of retinal, and rotation of the side chain of L93^{BR}, which are coupled with the vertical movement of a water molecule from the EC to the CP side [36]. Hence, the structural perturbation of helix C with the

mutation-induced interhelical interaction change between D92^{ARII} and C218^{ARII} might cause the change in the CP region dynamics for the early photoproducts K and/or L, resulting in effects on the kinetics of the formation and/or decay of these states. An example of an indirectly important role for an interhelical interaction in this function was previously reported in BR as well [37]. Perálvarez-Marín *et al.* reported that D115^{BR} on helix D forms an interhelical H-bond with T90^{BR} on helix C, and the disruption of the H-bond by the replacement of D115^{BR} or T90^{BR} to Ala renders the deprotonation of D96^{BR} during the photocycle impossible via the abolishment of the proper dynamics of helix C [37].

The most important effect of C218^{ARII} replacement on the photoreaction was found in the second half of the photocycle. A major difference in the photocycles of the mutants was the restrained N-to-O transition in C218^{ARII} mutants compared with the wild-type protein (Figs. 3 and 5). The replacement of C218^{ARII} delayed the proton uptake upon N-to-O transition similarly for both mutants (Fig. 6) regardless of the polarity of the introduced residues (hydrophobic alanine or hydrophilic serine), suggesting that the retardation of N-decay by the replacement of C218^{ARII} may not be merely attributed to a decrease in the proton conductivity of the CP channel. There are three conceivable factors that may induce the slowing of the N-to-O transition. The most feasible reason is the low proton affinity of D92^{ARII} upon its reprotonation, hampering the quick uptake of a proton from the CP surface. In fact, in the T46V^{BR} mutant, which exhibited a slower N-decay similar to the present case, it was considered that the cause of the prolonged lifetime of N was the lowering of the pK_a of D96^{BR} in the photolyzed state with the abolishment of the interaction with T46^{BR} [15,38]. To investigate whether the similar decrease in the pK_a of D92^{ARII} was caused with the

replacement of C218^{ARII}, we evaluated the pK_a values of D92^{ARII} during N-decay (O-formation), which was defined as p$K_{a,N}$, in the mutants. We estimated these p$K_{a,N}$ values from the pH dependence of the fraction of O. Here we assumed that the fraction of O is scarcely affected by the rate constants of the transitions prior to O-formation. In addition, it was assumed that the presence of a reverse reaction from O to N is negligible at acidic pH values (pH < ~7) because of relatively faster N-to-O transition. Under these assumptions, the fraction of O is theoretically determined by only rate constants of O-rise and -decay, and the fraction of pigment cycling [39]. The fraction of O can be roughly estimated from the maximum amplitudes of the absorbance changes at 610 nm (ΔA_{610}) in the latter time region from ~0.2 ms. Thus, the ΔA_{610}-normalized values in the wild-type ARII and two C218^{ARII} mutants were plotted as a function of pH in Fig. 7. Since the O-decay rate is almost independent of pH at least in the pH region from ~4 to ~7 (see Fig. S7), the pH dependent behavior of these plots may be only explained by the pH dependence of the N-to-O transition kinetics, which is governed by p$K_{a,N}$. As described below, this transition rate is regulated by other two factors (rates of switch of D92^{ARII} and reisomerization of retinal) as well as p$K_{a,N}$. These two factors are considered to be pH-independent and then the pH-dependence of the O-yield is determined only by the p$K_{a,N}$. From the plots in Fig. 7, the p$K_{a,N}$ values for the wild-type, C218A^{ARII}, and C218S^{ARII} were estimated to be 6.1, 5.3, and 4.7, respectively, whose magnitudes were in the order of the wild-type > C218A^{ARII} > C218S^{ARII}. We previously determined the pK_a value of D92^{ARII} in the wild-type upon H^+-uptake (N-decay) to be either 5.9 or 6.3 based on experimental results using the ITO method [22]. The close equality to the previous value indicates validity of the estimation by the present method. The order of the magnitudes of the p$K_{a,N}$ values among three proteins correlates well

with that of the turnover rates of their photocycles (see Fig. 2 or Table 1). During N-decay, the proton uptake occurs concurrently with the protonation of deprotonated $D92^{ARII}$. Thus, the proton affinity of $D92^{ARII}$ at N ($pK_{a,N}$) is one of the effective factors for the N-decay which is the rate determining step of the recovery to the initial state at neutral and above pH.

Although the changes of the $D92^{ARII}$-$C218^{ARII}$ interaction by the replacements of $C218^{ARII}$ affected the pK_a of $D92^{ARII}$ during N-decay, it is not clear whether $C218^{ARII}$ regulates the pK_a of $D92^{ARII}$ at the photolyzed state in the same way as $T46^{BR}$ because the abolishment of the H-bond ($C218A^{ARII}$) caused the prolongation of the lifetime of N similar to $T46V^{BR}$, but did not seem to induce much influence on the M-to-N transition (see Fig. 5Ab). In contrast, $T46V^{BR}$ led to more rapid M-decay as well as the delay of N-decay, resulting in the lack of observation of slow M-decay components by disappearance of the M-N quasi-equilibrium [15,38]. Therefore, we suppose that the perturbation of the H-bond of $D92^{ARII}$ with $C218^{ARII}$ might affect the $D92^{ARII}$-$N45^{ARII}$ interaction, which led to the change of the pK_a of $D92^{ARII}$ indirectly.

The second possible determinant for the N-decay kinetics may be the accessibility change of $D92^{ARII}$ between SB and the CP bulk [40]. In the case of BR, $D96^{BR}$ connects to SB but not the intracellular medium upon the M-to-N transition, blocking the misdirected migration of a proton of $D96^{BR}$ towards the CP bulk. At the next stage (upon the transition between two N-states (N_1 and N_2) [41,42]), this connection changes into the CP surface to take up a proton from the cytosol. Owing to this switching mechanism, the back-flow of a proton from PSB to $D96^{BR}$ is prevented, although the "switch-off" of the connection between PSB and $D96^{BR}$ is essentially achieved by the inversion of the pK_a values in these two residues. Thus, the accessibility-switching

machinery of $D96^{BR}$ may assist the efficient reprotonation of $D92^{ARII}$ from the CP bulk at the N-state and facilitate the subsequent transition from N (13-*cis*) to O (all-*trans*). A second factor may be the change in the interaction between $D92^{ARII}$ and $C218^{ARII}$, which may be involved in the accessibility switch of $D92^{ARII}$ at N-state.

The third possible factor is the rate of thermal reisomerization of retinal after reprotonation of $D92^{ARII}$. This rate could be also affected by the replacement of $C218^{ARII}$.

Considering three possible determinants for N-decay described above, the transition from M to O in ARII may be summarized as follows:

(1) Proton transfer from protonated $D92^{ARII}$ to SB ($M \rightarrow N_1$).

(2) Accessibility switch of deprotonated $D92^{ARII}$ facing SB into the CP bulk and formation of connectivity with the external media, which are caused by the influx of water with the conformational change in the CP channel ($N_1 \rightarrow N_1$').

(3) Formation of the below dissociation equilibrium: $D92^- + H_2O \rightleftarrows D92H + OH^-$ (N_1' $\leftrightarrow$ N_2). The presence of water molecules may originate from the (further) opening of helix F. The position of this equilibrium depends on $pK_{a,N}$ and pH around $D92^-$, which is assumed to be that of the CP medium.

(4) Protonated $D92^{ARII}$ (D92H) facilitates the isomerization of retinal from 13-*cis* to all-*trans*, implying that N_2 transforms to O via D92H ($N_2 \rightarrow O$). This transition occurs with retaining the equilibrium between N_1' and N_2. Thus, during the transition of N_1' to N_2, OH^- is produced and goes out to the CP medium, resulting in the alkalization in the medium (H^+-uptake).

For representing the N → O transition (processes (2)-(4) in the above scheme), here we introduced the following approximation for the kinetics of the N-to-O transition mainly observed as the third decay component of ΔA_{400} (τ_3). Since the overall kinetics of N-decay is probably determined by three factors described above: i) the switching rate of D92^{ARII} (denoted as k_s), ii) the fraction of protonated D92^{ARII}, and iii) the rate of the *cis*-to-*trans* isomerization of retinal (denoted as k_i), this transition rate can be described by

$$k_3 = k_s \times \left(\frac{[\mathrm{D92H}]}{[\mathrm{D92H}] + [\mathrm{D92^-}]} \right) \times k_i$$

Since k_s and k_i are most probably independent of the external pH, the product of these denotes k_N. Then, this equation is rewrote to

$$k_3 = k_N \left[\frac{1}{1 + 10^{n_a(\mathrm{pH} - \mathrm{p}K_{a,N})}} \right]$$

where p$K_{a,N}$ represents the pK_a of D92^{ARII} upon the N-to-O transition as defined above. In this equation, k_N ($= k_s \cdot k_i$) is independent of the protonation state of D92^{ARII} and corresponds to the maximal N-decay rate as is similar to the equation proposed by Balashov *et al*. [39,40]. n_a stands for the Hill coefficient, which is relevant to the slope of the τ_3-plot. This equation can be also expressed using time constant τ as follows:

$$\tau_3 = \tau_N \left[1 + 10^{n_a(\mathrm{pH} - \mathrm{p}K_{a,N})} \right]$$

Under the condition of $pK_{a,N}$ << pH, which is satisfied in the τ_3-plots of three ARII proteins (see lower panels (b) in Fig. 5), the above presented function on τ_3 is approximated as

$$\tau_3 \approx \tau_N \times 10^{n_a(pH-pK_{a,N})} = \frac{\tau_N}{10^{n_a \times pK_{a,N}}} \times 10^{n_a \times pH}$$

Since the lower panels of Fig. 5 are plotted as logarithm of τ_3 versus pH, the values of $\log \frac{\tau_N}{10^{n_a \times pK_{a,N}}}$ should be estimated from the y-intercepts. In addition, the slopes are almost equal among three proteins. Therefore, the shifts of y-axis originate from the difference of the y-intercept values. We calculated the τ_N values in three proteins using respective y-intercepts, n_a (slope), and $pK_{a,N}$ values determined from Fig. 7 (assuming the pH-independency of $pK_{a,N}$). The differences of the τ_N values between the wild-type and mutants, $\frac{\tau_{N,C218A}}{\tau_{N,wild\text{-}type}}$ and $\frac{\tau_{N,C218S}}{\tau_{N,wild\text{-}type}}$ were estimated to be ca. 2.0 and 2.8, respectively. According to the above definition ($k_N = k_s \cdot k_i$), τ_N (=$1/k_N$) signifies a constant including the time constants of the switch of $D92^{ARII}$ (denoted as τ_s) and reisomerization of retinal (denoted as τ_i). Therefore, these differences may reflect the delay of either the switch in $D92^{ARII}$ or reisomerization of retinal (or both) by the replacements of $C218^{ARII}$.

As described above, we showed that there are main two factors for the slowness of the photocycle rates (especially the slow decay of N-intermediate), which are caused by the changes of $pK_{a,N}$ and τ_N, respectively. If the H^+-uptake upon the N_1-to-N_2 transition is due only to the pK_a change of $D92^{ARII}$ at N, the rates of photocycle at acidic pH where

protons are in abundance should be the same between the wild-type and mutants. However, it was not the case (Fig. 4). Hence, this implies that not only the change of $pK_{a,N}$ but also change of τ_N (pH-independent factor) contributes to the delay of N-decay with the replacement of $C218^{ARII}$ even under lower pH conditions. Thus, the delayed N-decay of mutants compared to that of wild-type resulted in the slower turnover rates of mutants in all pH range.

As described above, the replacement of $C218^{ARII}$ changed τ_N composed of both τ_s and τ_i. The change of τ_i may imply the modulation of the rate of the conformational change leading to the delay of the configuration change of retinal.

Although the detailed molecular mechanism for switching of the proton donor between two N-substates has not yet been clearly defined even in the most well-known BR, the presence of a hydrophobic gate formed in the CP domain may be one of key components. $D96^{BR}$ in the CP-side of the channel is surrounded by hydrophobic residues, such as $F42^{BR}$, $I45^{BR}$, $L92^{BR}$, $L95^{BR}$, $L97^{BR}$, $L99^{BR}$, $L100^{BR}$, and $L223^{BR}$ [43]. A hydrophobic barrier composed of these residues shields the inner space between SB and $D96^{BR}$ from the external CP aqueous phase. The opening of the intracellular segment with the outward tilt of helix F at the M-state leads to the internal hydration of the CP domain [44]. However, a proton uptake pathway remains functionally closed even in this state, limiting the solvent accessibility of $D96^{BR}$. Wang *et al.* performed an *in silico* study using the X-ray crystal structure of a N-state-mimic $D96G/F171C/F219L^{BR}$ triple mutant [43]. Based on their computational results, they proposed that the deprotonation of $D96^{BR}$ along with the M-to-N transition catalyzes the further opening of the proton uptake pathway in the CP-side of the channel at the following N-state [43]. Thus, it may be predictable that the deprotonation of $D96^{BR}$ acts

as a switch to open the hydrophobic gate and change its own accessibility.

Most of the above described residues in BR are conserved in ARII. However, one of the residues in the intracellular hydrophobic cavity ($L223^{BR}$) is replaced by $C218^{ARII}$. Thus, $C218^{ARII}$ may not be irrelevant to the function of the hydrophobic CP gate as an accessibility switch of $D92^{ARII}$. If it is the case, it would be unclear why $C218^{ARII}$, which is missing in BR, is utilized for the switching of $D92^{ARII}$. The precise cause for this is unknown, but one of the conceivable reasons may be the lack of an amino-acid residue with a bulky group on its side chain at the end of the cavity. In BR, an aromatic ring of $F42^{BR}$ is located between $D96^{BR}$ and the CP surface that functions as a hydrophobic lid to separate $D96^{BR}$ from the CP media. Therefore, it has been hypothesized that $F42^{BR}$ is important for regulating the accessibility to the CP aqueous space [45,46]. According to the model by Wang *et al.*, it is likely that the phenyl ring of $F42^{BR}$ is displaced along with the deprotonation of $D96^{BR}$, facilitating the opening of the gate and the influx of water into the CP domain upon N-decay [43]. However, the corresponding residue in ARII is $A41^{ARII}$, whose side chain's volume is small (Fig. 1B); consequently, the gating control in ARII may be insufficient, unlike BR. Thus, the H-bond between $D92^{ARII}$ and $C218^{ARII}$ may serve as an alternative switch for compensating for the absence of the gating function by $F42^{BR}$. From this viewpoint, it may be noteworthy that this unique cysteine residue is not conserved in another homologue, ARI, which shows a slower photocycle [21]. The pH-dependent second slower phase of M-decay in ARI, mainly reflecting the conversion from the MN-quasi-equilibrium to O, was even slower than the N-decay rate of ARII [21]. ARI also lacks a residue corresponding to $F42^{BR}$ (replaced by $T44^{ARI}$). Therefore, together with the absence of phenolic lid in the CP region, the lack of the Asp-Cys interhelical

interaction may further decelerate the photocycle of ARI.

The FTIR studies by Heberle and colleagues implied the existence of a functional Asp-Cys ($D156^{ChR2}$-$C128^{ChR2}$) interaction in ChR2 [24], although the presence of a direct Asp-Cys H-bond was not observed in the crystal structure of a channelrhodopsin C1C2 chimera [47]. Most recently, Volkov *et al.* reported the crystal structures of the wild-type ChR2 and a $C128T^{ChR2}$ mutant [48]. According to these structures, the Asp-Cys interaction in the wild-type ChR2 was formed through a water molecule, whereas the Asp-Thr interaction in $C128T^{ChR2}$ was directly formed. Not only disabling mutations of the Asp-Cys interaction ($D156A^{ChR2}$ and $C128A^{ChR2}$) but also potentially conservative mutations ($C128S^{ChR2}$ and $C128T^{ChR2}$) commonly caused the prolongation of the lifetime of the photolyzed conductive state [49]. Together with our present study's findings, this demonstrates that the directly formed stronger interaction makes the gating control cease to function properly, as well as disruptions of the H-bond. Through the FTIR measurements by Heberle *et al.*, the interaction between $D156^{ChR2}$ and $C128^{ChR2}$ was observed at several photoproduct states, although the H-bonding strength was different from that of the dark state [24]. Unfortunately, it has not been yet determined how the H-bond changes at the photolyzed conductive states. Therefore, the detailed mechanism of gating control by the Asp-Cys interaction remains to be clarified with further spectroscopic or structural studies. Nevertheless, the present work implies that a weak interaction between Asp and Cys residues, which could be formed transiently, may function as the optimal switch for control of the gating in the CP-side of the channel.

5. Conclusions

Based on the solved X-ray crystal structure of ARII in the dark state [18], we previously identified the presence of a unique H-bond between $D92^{ARII}$ and $C218^{ARII}$ on different helices. In the present article, we examined how this H-bonding alteration with the replacement of $C218^{ARII}$ affected the photocycle and coupled proton transfer. Together with several kinetic changes of the photoproducts, both C-to-A replacement for abolishment of the H-bond and C-to-S replacement for conservation of the H-bond (but likely establishment of a stronger interaction) resulted in a delay of the turnover of the photocycle. The most crucial effect was observed in the N-to-O transition along with the reprotonation of $D92^{ARII}$ from the CP bulk, which was slowed down by these substitutions. As the putative role of the native weak Asp-Cys interhelical H-bond in ARII, we inferred that this interaction may be associated with i) the proper modulation of the pK_a of $D92^{ARII}$ and ii) the mechanism for switching of the accessibility of $D92^{ARII}$ and/or iii) reisomerization of retinal upon the N-O transition. However, the determination of the authentic role of this interaction and its detailed molecular mechanism awaits further studies.

Acknowledgements

We thank M. Inoue at RIKEN for plasmid construction. We also thank K. Date for his contributions at the early stages of this research. This work was supported by the Platform Project for Supporting in Drug Discovery and Life Science Research (Platform for Drug Discovery, Informatics, and Structural Life Science) from the Ministry of Education, Culture, Sports, Science, and Technology (MEXT) and Japan Agency for Medical Research and Development (AMED) to S.Y., the Targeted Protein Research Program from MEXT to S.Y., and grants from MEXT to K.S. (19770136) and N.K.

(22590049).

References

[1] J.L. Spudich, K.-H. Jung, in: W.R. Briggs, J.L. Spudich (Eds), Microbial rhodopsin: phylogenetic and functional diversity, In Handbook of photosensory receptors, Wiley-VCH Verlag, Weinheim, Germany, 2005, pp. 1-23.

[2] K.-H. Jung, The distinct signaling mechanisms of microbial sensory rhodopsins in archaea, eubacteria and eukarya, Photochem. Photobiol. 83 (2007) 63-69.

[3] O.P. Ernst, D.T. Lodowski, M. Elstner, P. Hegemann, L.S. Brown, H. Kandori, Microbial and animal rhodopsins: structures, functions, and molecular mechanisms, Chem. Rev. 114 (2014) 126-163.

[4] L.S Brown, Eubacterial rhodopsins - Unique photosensors and diverse ion pumps, Biochim. Biophys. Acta 1837 (2014) 553-561.

[5] J.L. Spudich, C.-S. Yang, K.-H. Jung, E.N. Spudich, Retinylidene proteins: structures and functions from archaea to humans, Annu. Rev. Cell Dev. Biol. 16 (2000) 365-392.

[6] M. Grote, M. Engelhard, P. Hegemann, Of ion pumps, sensors and channels - Perspectives on microbial rhodopsins between science and history, Biochim. Biophys. Acta 1837 (2014) 533-545.

[7] U. Haupts, J. Tittor, D. Oesterhelt, Closing in on bacterorhodopsin: progress in understanding the molecule, Ann. Rev. Biophys. Biomole. Struct. 28 (1999) 367-399.

[8] S. Subramaniam, R. Henderson, Crystallographic analysis of protein conformational changes in the bacteriorhodopsin photocycle, Biochim. Biophys. Acta 1460 (2000) 157-165.

[9] J. Heberle, Proton transfer reactions across bacteriorhodopsin and along the

membrane, Biochim. Biophys. Acta 1458 (2000) 135-147.

[10] J.K. Lanyi, Bacteriorhodopsin, Annu. Rev. Physiol. 66 (2004) 665-688.

[11] S. Száraz, D. Oesterhelt, P. Ormos, pH-induced structural changes in bacteriorhodopsin studied by Fourier transform infrared spectroscopy, Biophys. J. 67 (1994) 1706-1712.

[12] H. Luecke, B. Schobert, H.-T. Richter, J.-P. Cartailler, J.K. Lanyi, Structure of bacteriorhodopsin at 1.55 Å resolution, J. Mol. Biol. 291 (1999) 899-911.

[13] H. Luecke, B. Schobert, J.-P. Cartailler, H.T. Richter, A. Rosengarth, R. Needleman, J.K. Lanyi, Coupling photoisomerization of retinal to directional transport in bacteriorhodopsin, J. Mol. Biol. 300 (2000) 1237-1255.

[14] C. Zscherp, R. Schlesinger, J. Tittor, D. Oesterhelt, J. Heberle, *In situ* determination of transient pK_a changes of internal amino acids of bacteriorhodopsin by using time-resolved attenuated total reflection Fourier-transform infrared spectroscopy, Proc. Natl. Acad. Sci. USA 96 (1999) 5498-5503.

[15] A.K. Dioumaev, L.S. Brown, R. Needleman, J.K. Lanyi, Coupling of the reisomerization of the retinal, proton uptake, and reprotonation of Asp-96 in the N photointermediate of bacteriorhodopsin, Biochemistry 40 (2001) 11308-11317.

[16] S.P. Tsunoda, D. Ewers, S. Gazzarrini, A. Moroni, D. Gradmann, P. Hegeman, H^+-pumping rhodopsin from the marine alga *Acetabularia*, Biophys. J. 91 (2006) 1471-1479.

[17] S.-S. Lee, A.R. Choi, S.Y. Kim, H.-W. Kang, K.-H. Jung, J.-H. Lee, *Acetabularia* rhodopsin I is a light-stimulated proton pump, J. Nanosci. Nanotechnol. 11 (2011) 4596-4600.

[18] T. Wada, K. Shimono, T. Kikukawa, M. Hato, N. Shinya, S.Y. Kim, T. Kimura-Someya, M. Shirouzu, J. Tamogami, S. Miyauchi, K.-H. Jung, N. Kamo, S. Yokoyama, Crystal structure of the eukaryotic light-driven proton pumping rhodopsin, *Acetabularia* rhodopsin II, from marine alga, J. Mol. Biol. 411 (2011) 986-998.

[19] K.A. Lee, S.-S. Lee, S.Y. Kim, A.R. Choi, J.-H. Lee, K.-H. Jung, Mistic-fused expression of algal rhodopsins in *Escherichia coli* and its photochemical properties, Biochim. Biophys. Acta 1850 (2015) 1694-1703.

[20] K. Shimono, M. Goto, T. Kikukawa, S. Miyauchi, M. Shirouzu, N. Kamo, S. Yokoyama, Production of functional bacteriorhodopsin by an *Escherichia coli* cell-free protein synthesis system supplemented with steroid detergent and lipid, Protein Sci. 18 (2009) 2160-2171.

[21] M. Furuse, J. Tamogami, T. Hosaka, T. Kikukawa, N. Shinya, M. Hato, N. Ohsawa, S.-Y. Kim, K.-H. Jung, M. Demura, S. Miyauchi, N. Kamo, K. Shimono, T.

Kimura-Someya, S. Yokoyama, M. Shirouzu, Structural basis for the slow photocycle and late proton release in *Acetabularia* rhodopsin I from the marine plant *Acetabularia* acetabulum, Acta Crystallogr., Sect. D: Biol. Crystallogr. 71 (2015) 2203-2216.

[22] T. Kikukawa, K. Shimono, J. Tamogami, S. Miyauchi, S.Y. Kim, T. Kimura-Someya, M. Shirouzu, K.-H. Jung, S. Yokoyama, N. Kamo, Photochemistry of *Acetabularia* rhodopsin II from a marine plant, *Acetabularia acetabulum*, Biochemistry 50 (2011) 8888-8898.

[23] E.N. Spudich, G. Ozorowski, E.V. Schow, D.J. Tobias, J.L. Spudich, H. Luecke, A transporter converted into a sensor, a phototaxis signaling mutant of bacteriorhodopsin at 3.0 Å, J. Mol. Biol. 415 (2012) 455-463.

[24] M. Nack, I. Radu, M. Gossing, C. Bamann, E. Bamberg, G.F. von Mollard, J. Heberle, The DC gate in channelrhodopsin-2: crucial hydrogen bonding interaction between C128 and D156, Photochem. Photobiol. Sci. 9 (2010) 194-198.

[25] M. Sato, T. Kikukawa, T. Araiso, H. Okita, K. Shimono, N. Kamo, M. Demura, K. Nitta, Role of Ser130 and Thr126 in chloride binding and photocycle of *pharaonis* halorhodopsin, J. Biochem. 134 (2003) 151-158.

[26] I. Chizhov, D.S. Chernavskii, M. Engelhard, K.-H. Mueller, B.V. Zubov, B. Hess, Spectrally silent transitions in the bacteriorhodopsin photocycle, Biophys. J. 71 (1996) 2329-2345.

[27] M. Sato, M. Kubo, T. Aizawa, N. Kamo, T. Kikukawa, K. Nitta, M. Demura, Role of putative anion-binding sites in cytoplasmic and extracellular channels of *Natronomonas pharaonis* halorhodopsin, Biochemistry 44 (2005) 4775-4784.

[28] C. Hasegawa, T. Kikukawa, S. Miyauchi, A. Seki, Y. Sudo, M. Kubo, M. Demura, N. Kamo, Interaction of the halobacterial transducer to a halorhodopsin mutant engineered so as to bind the transducer: Cl^- circulation within the extracellular channel, Photochem. Photobiol. 83 (2007) 293-302.

[29] Y. Tateishi, T. Abe, J. Tamogami, Y. Nakao, T. Kikukawa, N. Kamo, M. Unno, Spectroscopic evidence for the formation of an N intermediate during the photocycle of sensory rhodopsin II (phoborhodopsin) from *Natronobacterium pharaonis*, Biochemistry 50 (2011) 2135-2143**.**

[30] R.R. Birge, Nature of the primary photochemical events in rhodopsin and bacteriorhodopsin, Biochim. Biophys. Acta 1016 (1990) 293-327.

[31] J. Tamogami, T. Kikukawa, S. Miyauchi, E. Muneyuki, N. Kamo, A tin oxide transparent electrode provides the means for rapid time-resolved pH measurements: application to photoinduced proton transfer of bacteriorhodopsin and proteorhodopsin, Photochem. Photobiol. 85 (2009) 578-589.

[32] B. Becher, J.Y. Cassim, Effects of light adaptation on the purple membrane

structure of *Halobacterium halobium*, Biophys. J. 16 (1976) 1183-1200.

[33] J. Tamogami, T. Kikukawa, T. Nara, M. Demura, T. Kimura-Someya, M. Shirouzu, S. Yokoyama, S. Miyauchi, K. Shimono, N. Kamo, Existence of two O-like intermediates in the photocycle of *Acetabularia* rhodopsin II, a light-driven proton pump from a marine alga, Biophys. Physicobiol. 14 (2017) 49-55.

[34] J. Tamogami, K. Sato, S. Kurokawa, T. Yamada, T. Nara, M. Demura, S. Miyauchi, T. Kikukawa, E. Muneyuki, N. Kamo, Formation of M‑like intermediates in proteorhodopsin in alkali solutions (pH ≥ ~8.5) where the proton release occurs first in contrast to the sequence at lower pH, Biochemistry 55 (2016) 1036-1048.

[35] A. Miller, D. Oesterhelt, Kinetic optimization of bacteriorhodopsin by aspartic acid 96 as an internal proton donor, Biochim. Biophys. Acta 1020 (1990) 57-64.

[36] T. Kouyama, T. Nishikawa, T. Tokuhisa, H Okumura, Crystal structure of the L intermediate of bacteriorhodopsin: evidence for vertical translocation of a water molecule during the proton pumping cycle, J. Mol. Biol. 335 (2004) 531-546.

[37] A. Perálvarez-Marín, V.A. Lórenz-Fonfría, J.-L. Bourdelande, E. Querol, H. Kandori, E. Padrós, Inter-helical hydrogen bonds are essential elements for intra-protein signal transduction: the role of Asp115 in bacteriorhodopsin transport function, J. Mol. Biol. 368 (2007) 666-676.

[38] L.S. Brown, L. Zimányi, R. Needleman, M. Ottolenghi, J.K. Lanyi, Photoreaction of the N intermediate of bacteriorhodopsin, and its relationship to the decay kinetics of the M intermediate, Biochemistry 32 (1993) 7679-7685.

[39] S.P. Balashov, M. Lu, E.S. Imasheva, R. Govindjee, T.G. Ebrey, B. Othersen III, Y. Chen, R.K. Crouch, D.R. Menick, The proton release group of bacteriorhodopsin controls the rate of the final step of its photocycle at low pH, Biochemistry 38 (1999) 2026-2039.

[40] S.P. Balashov, Protonation reactions and their coupling in bacteriorhodopsin, Biochim. Biophys. Acta 1460 (2000) 75-94.

[41] J.B. Ames, R.A. Mathies, The role of back-reactions and proton uptake during the N → O transition in bacteriorhodopsin's photocycle: a kinetic resonance Raman study, Biochemistry 29 (1990) 7181-7190.

[42] L. Zimányi, Y. Cao, R. Needleman, M. Ottolenghi, J.K. Lanyi, Pathway of proton uptake in the bacteriorhodopsin photocycle, Biochemistry 32 (1993) 7669-7678.

[43] T. Wang, A.O. Sessions, C.S. Lunde, S. Rouhani, R.M. Glaeser, Y. Duan, M.T. Facciotti, Deprotonation of D96 in bacteriorhodopsin opens the proton uptake pathway, Structure 21 (2013) 290-297.

[44] Y Cao, G. Váró, M. Chang, B. Ni, R. Needleman, J.K. Lanyi, Water is required for

proton transfer from aspartate-96 to the bacteriorhodopsin Schiff base, Biochemistry 30 (1991) 10972-10979.

[45] B. Schätzler, N.A. Dencher, J. Tittor, D. Oesterhelt, S. Yaniv-Checover, E. Nachliel, M. Gutman, Subsecond proton-hole propagation in bacteriorhodopsin, Biophys. J. 84 (2003) 671-686.

[46] R. Friedman, E. Nachliel, M. Gutman, The role of small intraprotein cavities in the catalytic cycle of bacteriorhodopsin, Biophys. J. 85 (2003) 886-896.

[47] H.E. Kato, F. Zhang, O. Yizhar, C. Ramakrishnan, T. Nishizawa, K. Hirata, J. Ito, Y. Aita, T. Tsukazaki, S. Hayashi, P. Hegemann, A.D. Maturana, R. Ishitani, K. Deisseroth, O. Nureki, Crystal structure of the channelrhodopsin light-gated cation channel, Nature 482 (2012) 369-374.

[48] O. Volkov, K. Kovalev, V. Polovinkin, V. Borshchevskiy, C. Bamann, R. Astashkin, E. Marin, A. Popov, T. Balandin, D. Willbold, G. Büldt, E. Bamberg, V. Gordeliy, Structural insights into ion conduction by channelrhodopsin 2, Science 358 (2017) eaan8862.

[49] C. Bamann, R. Gueta, S. Kleinlogel, G. Nagel, E. Bamberg, Structural guidance of the photocycle of channelrhodopsin-2 by an interhelical hydrogen bond, Biochemistry 49 (2010) 267-278.

Figure legends

Figure 1: Structural aspect in the CP-side channel of ARII. (A) Overall structure of ARII monomer based on the previously solved X-ray crystal structure at 3.2-Å resolution (PDB code: 3AM6) [18]. (B) Close-up view of the CP transmembrane region

surrounded by a blue broken line in panel (A). The residues forming two types of interhelical interactions with $D92^{ARII}$ are shown together with several neighboring residues. The corresponding residues in BR are in parentheses. (C) Formation of hydrogen bond between $D92^{ARII}$ and $C218^{ARII}$.

Figure 2: Time-dependent flash-induced absorbance changes in the wild-type (A), $C218A^{ARII}$ (B), and $C218S^{ARII}$ (C). The data at three selected wavelengths (400, 530, and 610 nm) are shown. The observed and regression curves by global fitting analysis are represented in gray and black lines, respectively. Experimental conditions were as follows: the media included 400 mM NaCl, 0.05% DDM, and 6 mixed buffers (citrate, MES, HEPES, MOPS, CHES, CAPS, at 10 mM each). The pH was 7.0. The temperature was set to 20°C. The corresponding figure for the wild-type was drawn from the obtained dataset in a previous publication [22].

Figure 3: Absorption spectra of photointermediates in kinetic photoproduct P_i-states. Respective spectra of P_i (i=1-4 (mutants) or -5 (wild-type)) calculated by global fitting for the wild-type (A), $C218A^{ARII}$ (B), and $C218S^{ARII}$ (C) are shown separately in panels (a)-(e) in the order of their appearance in the scheme. The observed data of respective P_i-spectra are shown in filled circles, while those of the dark-state (P_0)-spectra are shown in gray continuous lines. The bold continuous and thin broken lines represent the fitting curves generated from skewed Gaussian functions for the observed data and putative spectra of the photocycle intermediates in each P_i-state estimated from the fitting, respectively.

Figure 4: Flash-induced absorbance changes for C218A^{ARII} (A) and C218S^{ARII} (B) at different pH values. The pH of the medium was titrated from 4.0 to 9.0 every 0.5 units. The full data are shown in Fig. S3 (A, C218A^{ARII} and B, C218S^{ARII}). Of these data, representative data at four pH values, pH 4.0 (a), 6.0 (b), 8.0 (c), and 9.0 (d), are shown. The noisy gray and smooth black lines represent the observed and fitting curves, respectively. The simultaneous multiexponential fitting for three absorption changes was performed using a function with four exponential terms, with the exception of three datasets for C218A^{ARII} at pH 4.5, 5.0, and 5.5, which required five terms. For comparison, the corresponding data of the wild-type, which were quoted from our previous article [22], were shown as dotted (400 nm), broken (520 nm), and chain (610 nm) lines.

Figure 5: pH dependence of the decay of the absorbance changes at 400 nm in C218A^{ARII} (A) and C218S^{ARII} (B). The upper panels (a) show the different decay patterns of the ΔA_{400} signals at three pH values. The noisy and smooth lines represent the observed and multiexponential fitting curves, respectively. The lower panels (b) show the plots of the multiple decay time constants against the pH. The inset of the left panel shows the corresponding plots for the wild-type. The plots of τ_1, τ_2, and τ_3 are shown as closed squares, circles, and triangles, respectively. The τ_4 and τ_5 values stand for the time constants of the rise and decay of a M-like photoproduct (M_a), which are shown in open and closed diamonds, respectively (also see the Supplementary materials). For comparison, the pH-dependence of τ_3 in the wild-type is shown as a dashed line.

Figure 6: Photoinduced proton uptake and release in C218A^{ARII} (A) and C218S^{ARII} (B). The scattered signals in the respective panels represent the observed ITO signals at pH 8.5. Since these signals contained significant noise due to their relatively small amplitudes, smoothing lines are shown for the purpose of making traces of the changes easier. Gray solid lines in each panel represent the appropriately multiplied signal of the wild-type at the same pH value. Experiments were performed in the media containing 400 mM NaCl and the aforementioned six buffers at 1 mM each. The temperature was approximately 25°C (room temperature).

Figure 7: Estimation of pK_a of D92^{ARII} during N-to-O transition from pH dependence of O-yield. The maximum amplitudes of the absorbance changes at 610 nm in the wild-type (filled squares), C218A^{ARII} (filled circles), and C218S^{ARII} (empty circles) were plotted against pH. The plotted values for C218A^{ARII} and C218S^{ARII} were obtained from the data in Fig. S3, whereas those of the wild-type were obtained from the data in ref. [22]. To avoid the change of the fraction of O with the change of the functional pigment, which could be caused by e.g. protonation of a counterion (D81^{ARII}) of PSB at lower pH or deprotonation of PSB at higher pH in the dark, the values of O-yields were normalized to the maximum amplitude of M produced at respective pH values. The unit of the y-axis values is arbitrary. The plotted values were fitted by the Henderson-Hasselbalch equation with a single pK_a value: $f_O(\mathrm{pH}) = A\left[\frac{1}{1+10^{n_a(\mathrm{pH}-\mathrm{p}K_{a,N})}}\right]$, where A, n_a, and p$K_{a,N}$ are the scaling constant for the amplitude, Hill coefficient, and pK_a of D92^{ARII} during N-decay, respectively. The values of the slopes of the τ_3-plots in respective proteins (wild-type, 0.55; C218A^{ARII}, 0.60;

C218S^{ARII}, 0.64) were used for n_a.

Table 1: Comparison of lifetimes of P_i-states among ARII and two C218^{ARII} mutants at

pH 7.0[1)]

	P_1	P_2	P_3	P_4	P_5
ARII (WT)[2)]	0.015	0.097	0.77	7.96	20.9
C218A	0.017	0.120	4.95	51.8	-
C218S	0.009	0.059	4.01	261.7	-

[1)]The unit of all time constant values is milliseconds.

[2)]The corresponding values of the wild-type were cited from a previous paper [22].

Figure 1

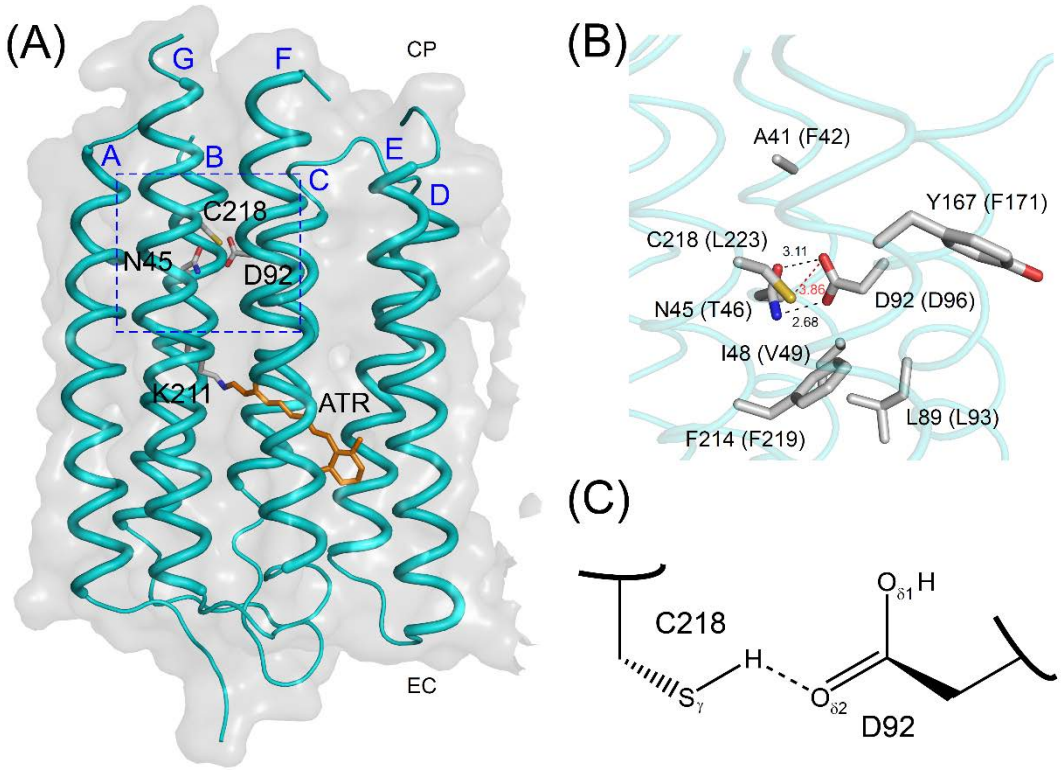
(A)
G
F
CP
A
B
C
E
D
C218
N45
D92
K211
ATR
EC
(B)
A41 (F42)
Y167 (F171)
C218 (L223)
3.11
3.86
N45 (T46)
D92 (D96)
2.68
I48 (V49)
L89 (L93)
F214 (F219)
(C)
C218
H
D92

Figure 2

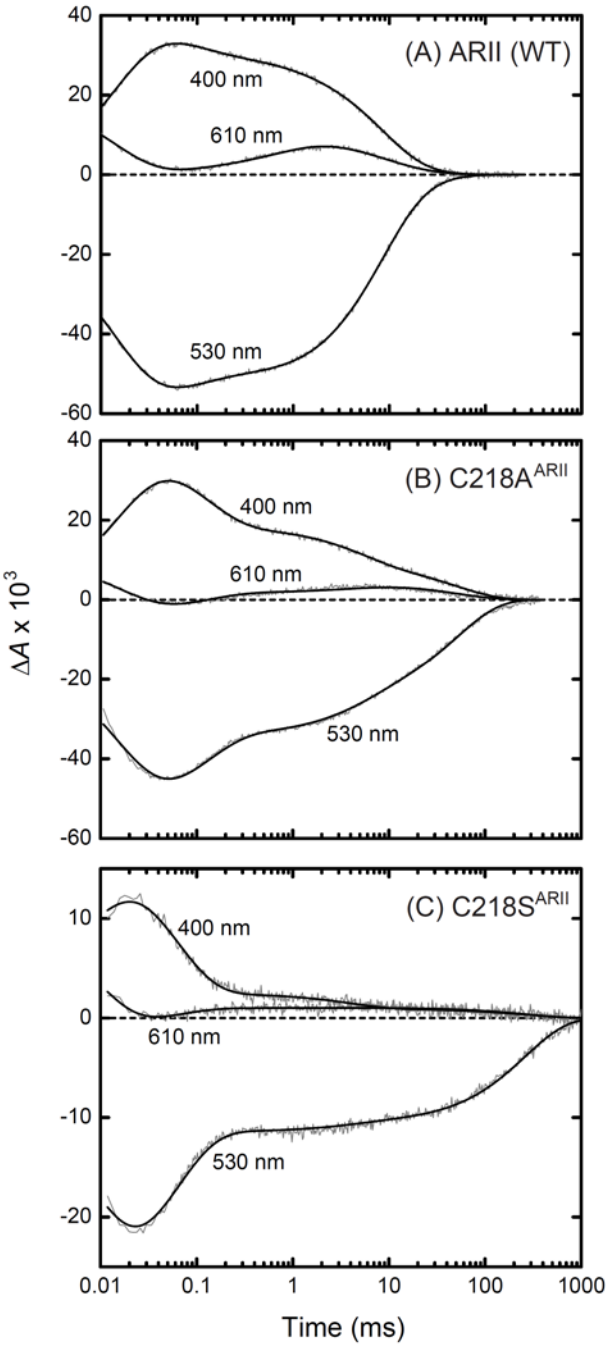
(A) ARII (WT)
400 nm
610 nm
530 nm
(B) C218A^ARII
400 nm
610 nm
530 nm
(C) C218S^ARII
400 nm
610 nm
530 nm
ΔA x 10^3
Time (ms)
40
20
0
-20
-40
-60
10
-10
-20
0.01
0.1
1
10
100
1000

Figure 3

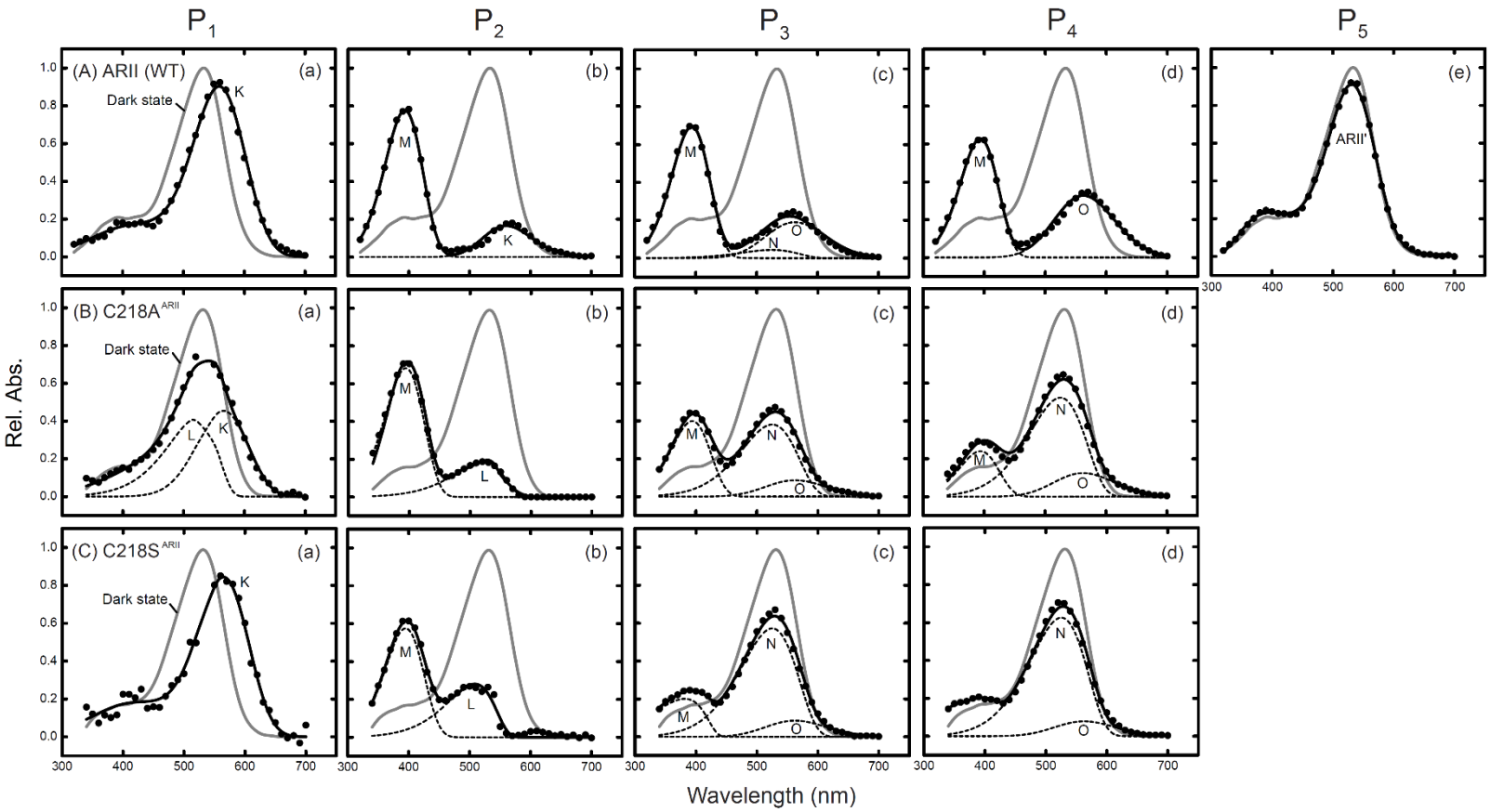
P1
P2
P3
P4
P5
(A) ARII (WT)
(B) C218A^ARII
(C) C218S^ARII
(a)
(b)
(c)
(d)
(e)
Dark state
K
L
M
N
O
ARII*
Rel. Abs.
Wavelength (nm)

Figure 4

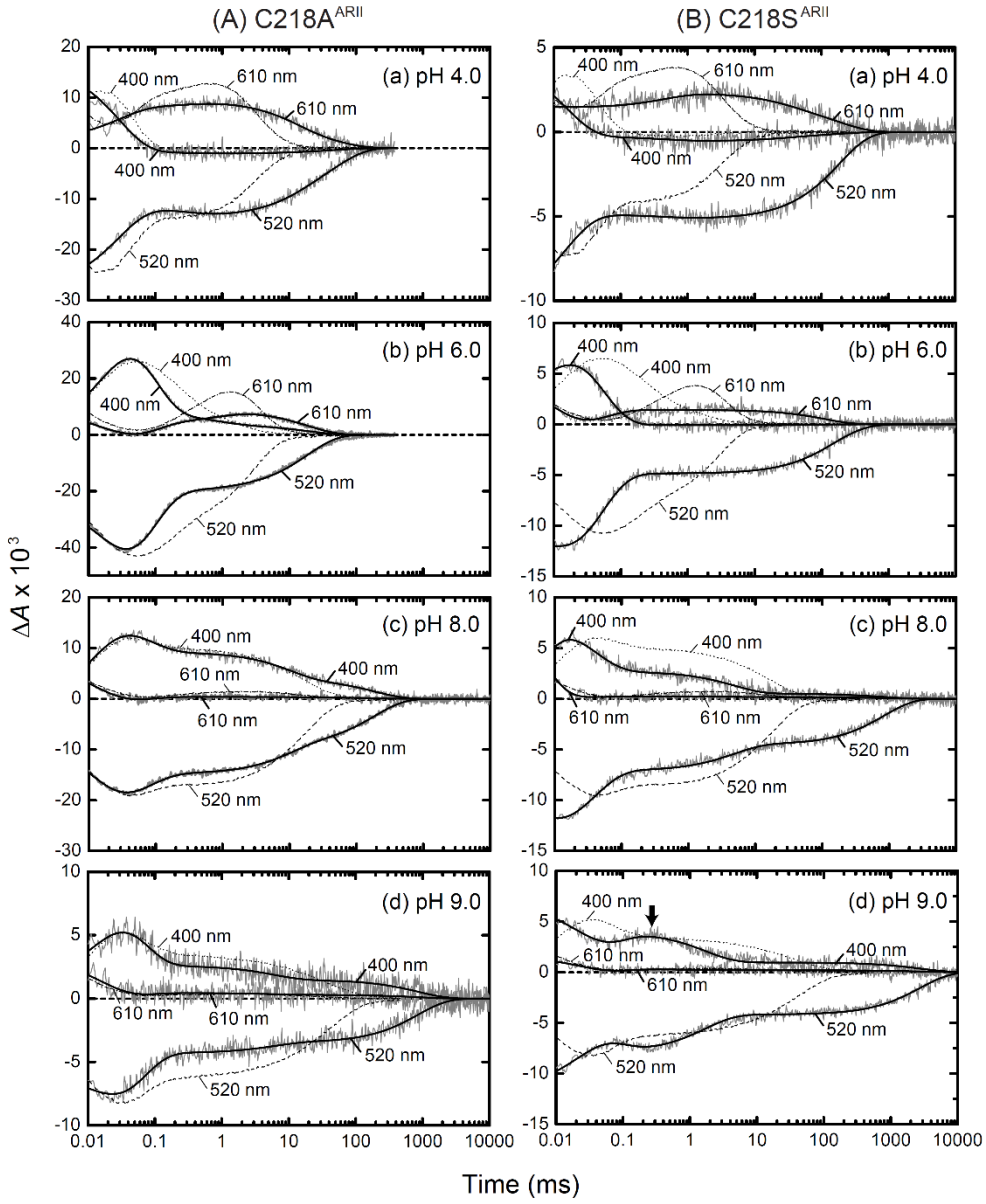
(A) C218A^ARII
(B) C218S^ARII
(a) pH 4.0
(b) pH 6.0
(c) pH 8.0
(d) pH 9.0
400 nm
610 nm
520 nm
ΔA x 10^3
Time (ms)

Figure 5

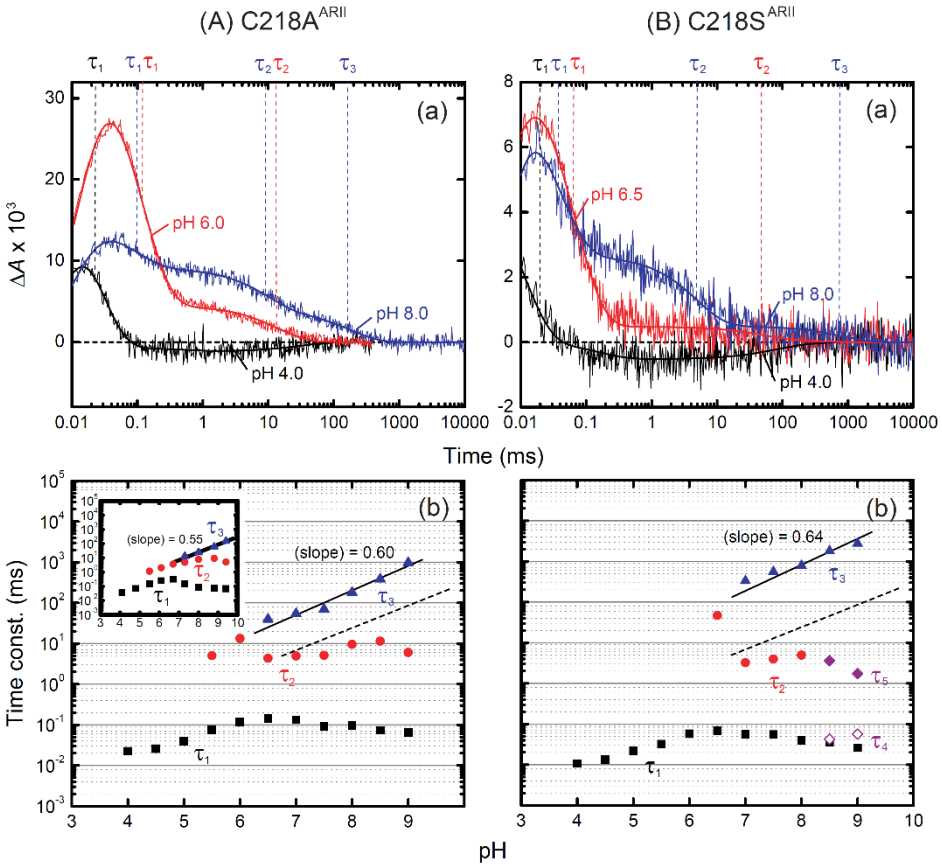
(A) C218A^ARII
(B) C218S^ARII
(a)
(b)
ΔA x 10^3
pH 6.0
pH 8.0
pH 4.0
pH 6.5
Time (ms)
Time const. (ms)
(slope) = 0.55
(slope) = 0.60
(slope) = 0.64
pH

Figure 6

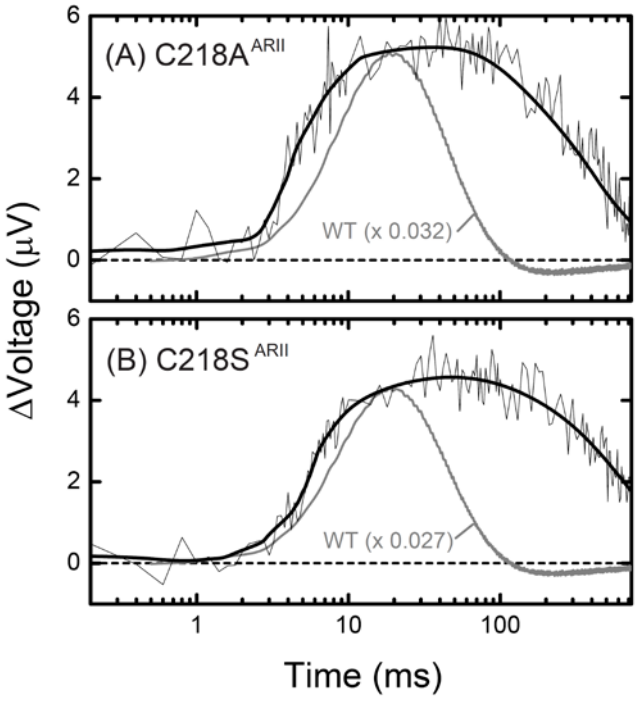
(A) C218A ARII
WT (x 0.032)
(B) C218S ARII
WT (x 0.027)
ΔVoltage (μV)
Time (ms)
6
4
2
0
1
10
100

Figure 7

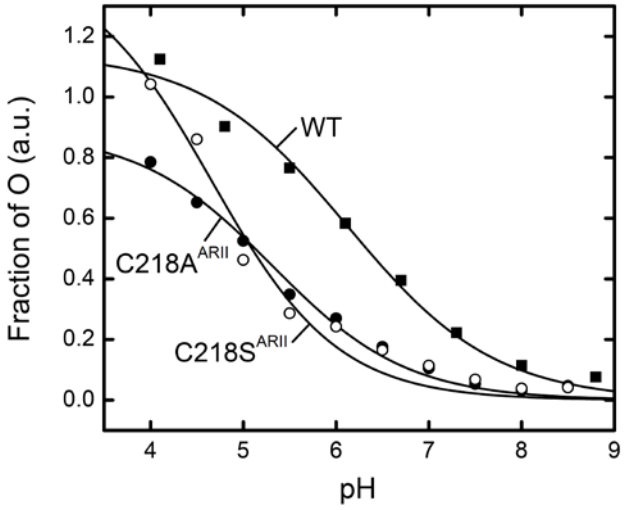
Fraction of O (a.u.)
pH
WT
C218A^ARII
C218S^ARII
1.2
1.0
0.8
0.6
0.4
0.2
0.0
4
5
6
7
8
9

Supplementary Materials

Interhelical interactions between D92 and C218 in the cytoplasmic domain regulate proton uptake upon N-decay in the proton transport of *Acetabularia* rhodopsin II

Jun Tamogami, Takashi Kikukawa, Keisuke Ohkawa, Noboru Ohsawa, Toshifumi Nara, Makoto Demura, Seiji Miyauchi, Tomomi Kimura-Someya, Mikako Shirouzu, Shigeyuki Yokoyama, Kazumi Shimono and Naoki Kamo

Table S1: Parameters of the skewed Gaussian fit for P_i-spectra in Fig. 3

	$\lambda_{1,\,max}$ [nm]	$A_{1,\,max}$	ρ_1	$\Delta\nu_1$ [cm^{-1}]	$\lambda_{2,\,max}$ [nm]	$A_{2,\,max}$	ρ_2	$\Delta\nu_2$ [cm^{-1}]	$\lambda_{3,\,max}$ [nm]	$A_{3,\,max}$	ρ_3	$\Delta\nu_3$ [cm^{-1}]
(A) ARII (WT)												
P_0 (dark state)	534											
P_1	417 (β-band?)	0.16	1.5	9333	560 (K)	0.90	1.3	3254	-	-	-	-
P_2	394 (M)	0.79	1.5	4801	560 (K)	0.17	1.1	2986	-	-	-	-
P_3	394 (M)	0.70	1.5	4801	526 (N)	0.04	1.8	4165	562 (O)	0.19	1.1	3652
P_4	394 (M)	0.64	1.5	4801	562 (O)	0.33	1.1	3652	-	-	-	-
P_5	392 (β-band?)	0.23	0.8	7908	532(ARII')	0.87	1.3	3224	-	-	-	-
(B) $C218A^{ARII}$												
P_0 (dark state)	533											
P_1	417 (β-band?)	0.09	1.5	9333	522 (L)	0.42	2.0	3817	566 (K)	0.46	1.3	3098
P_2	394 (M)	0.69	1.5	4978	522 (L)	0.19	2.0	3817	-	-	-	-
P_3	394 (M)	0.41	1.5	4978	526 (N)	0.38	1.8	4165	562 (O)	0.09	1.1	3652
P_4	394 (M)	0.24	1.5	4978	526 (N)	0.53	1.8	4165	562 (O)	0.13	1.1	3652
(C) $C218S^{ARII}$												
P_0 (dark state)	532											
P_1	417 (β-band?)	0.18	1.5	9333	566 (K)	0.84	1.3	3098	-	-	-	-
P_2	395 (M)	0.58	1.5	4858	509 (L)	0.28	2.0	3817	-	-	-	-
P_3	382 (M)	0.20	2.5	4858	526 (N)	0.58	1.8	4165	562 (O)	0.09	1.1	3652
P_4	372 (M or β-band?)	0.16	2.9	10884	526 (N)	0.63	1.8	4165	562 (O)	0.08	1.1	3652

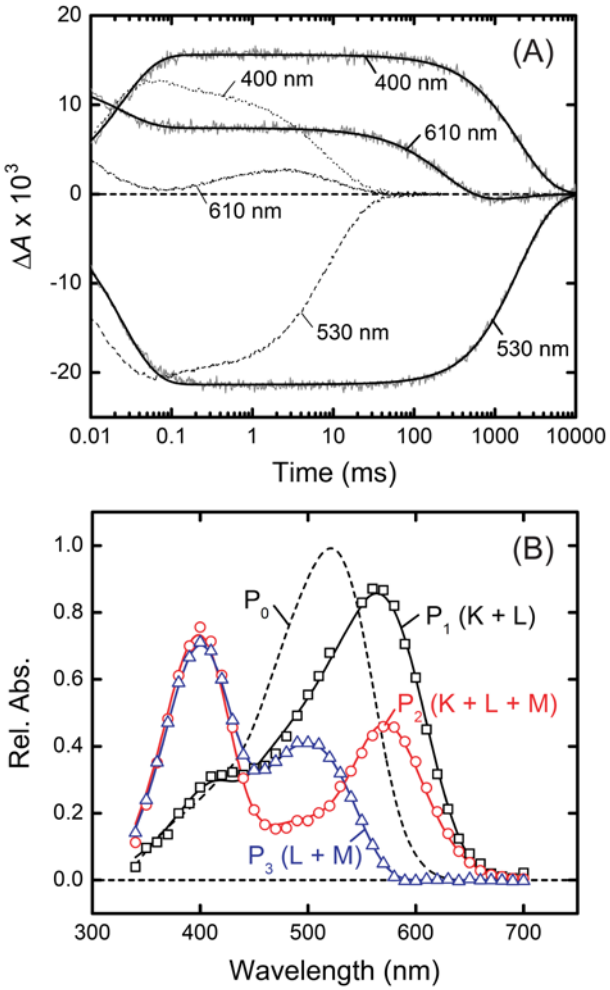

Figure S1: Photocycle of D92N[ARII]. (A) Flash-induced absorbance changes at three selected wavelengths (400, 530 and 610 nm). The observed signals are represented as gray noisy lines, while the regression curves by the global fitting are represented as black smooth lines. The wild-type data at the same pH are shown as dotted (400 nm), broken (530 nm), and chain (610 nm) lines. Through the global fitting, the lifetimes (decay time constants) of the three P-states were estimated as 0.024 ms for P_1, 238.7 ms for P_2, and 1970.4 ms for P_3, respectively. (B) Absorbance spectra of P_i-states (i=1-3) determined by the global fitting. The spectrum at the unphotolyzed state (P_0) having a λ_{max} at ca. 522 nm is shown as a black broken line. Measurements were performed under the same experimental conditions described in Fig. 2.

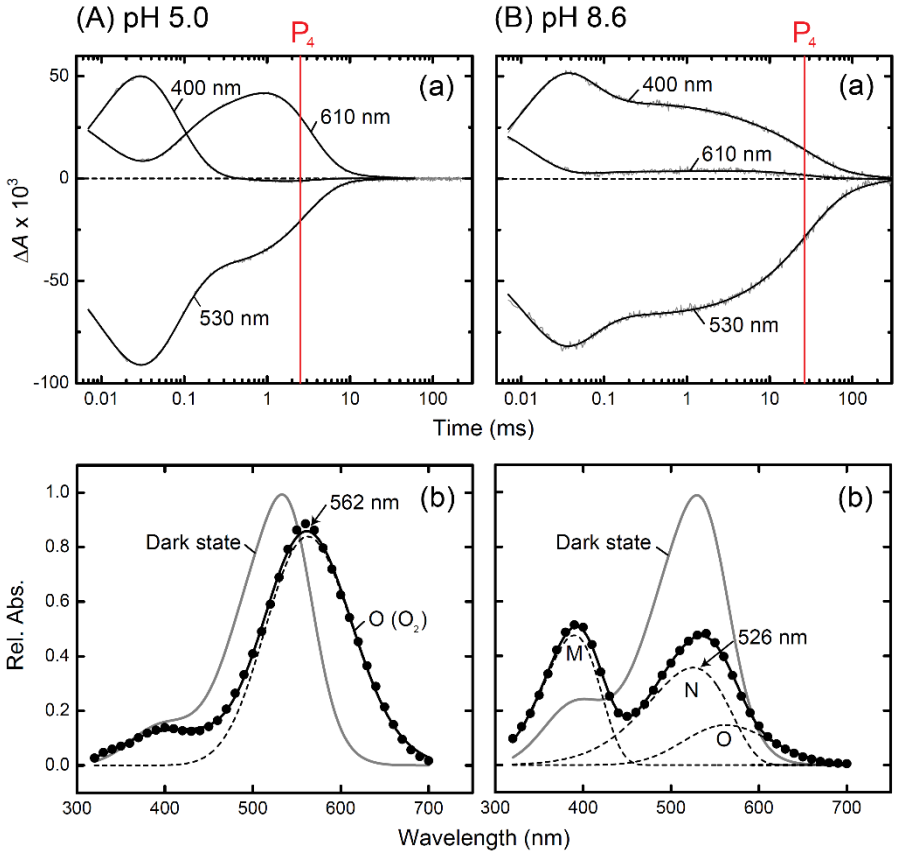

Figure S2: Estimation of O- and N-spectra. The presented data are from the previous results of the global fitting in the wild-type at pH 5.0 (A) and 8.6 (B) [S1]. The upper panels (a) show the absorbance changes (gray lines) at three wavelengths (400, 530, and 610 nm) together with the fitting curves (black lines). The vertical red lines in each panel exhibit the time constants of P_4-decay at respective pH values. The lower panels (b) show the results of the fitting analyses with the skewed Gaussian functions for the spectra of P_4. As described previously, the spectrum of P_4 at pH 5.0 contains only an absorption band of O (O_2) as a photoproduct [S2]. Therefore, the analysis for P_4-spectrum yielded an absolute spectrum of O (shown in a broken line). The spectral parameters of O estimated from the fitting were $\lambda_{max} = 562$ nm, $A_{max} = 0.84$, $\rho = 1.1$, and $\Delta\nu = 3652$ cm^{-1}. Another small absorbance band at the shorter spectral range (~300-450 nm) may be due to the β-band. The P_4-spectrum at pH 8.6 is in the

quasi-equilibrium of M, N, and O, where the N/O ratio is >1 because of the slower N-to-O transition at this pH. Thus, the analysis of the P_4-spectrum at pH 8.6 was performed by the function with three Gaussian bands. The calculated spectra of M, N, and O by the fitting are shown as broken lines. During the fitting, the spectral parameters of O, except A_{max}, were fixed to the same values estimated from the analysis for P_4 at pH 5.0. The estimated spectral parameters of N were $\lambda_{max} = 526$ nm, $A_{max} = 0.36$, $\rho = 1.8$, and $\Delta\nu = 4165$ cm^{-1}.

(A) C218A^{ARII}

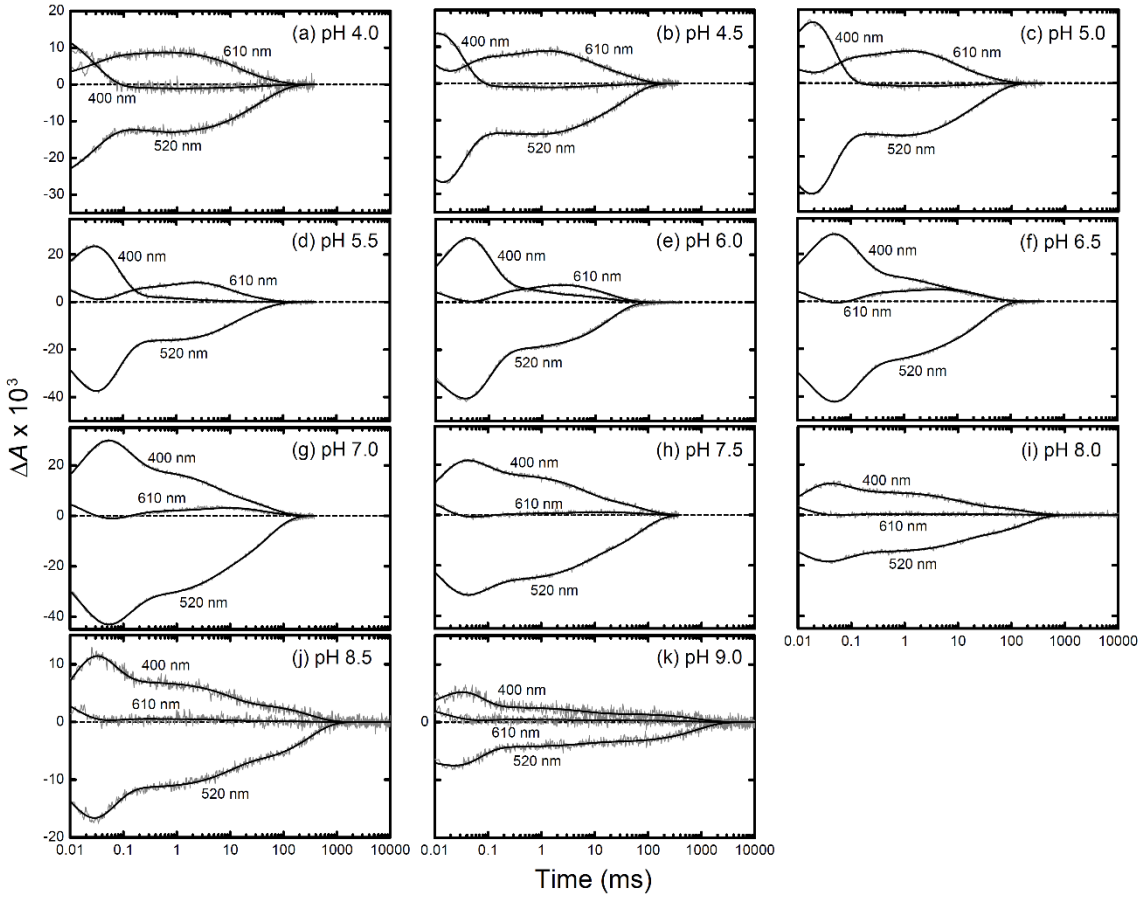
(a) pH 4.0
(b) pH 4.5
(c) pH 5.0
(d) pH 5.5
(e) pH 6.0
(f) pH 6.5
(g) pH 7.0
(h) pH 7.5
(i) pH 8.0
(j) pH 8.5
(k) pH 9.0
400 nm
610 nm
520 nm
ΔA x 10^3
Time (ms)

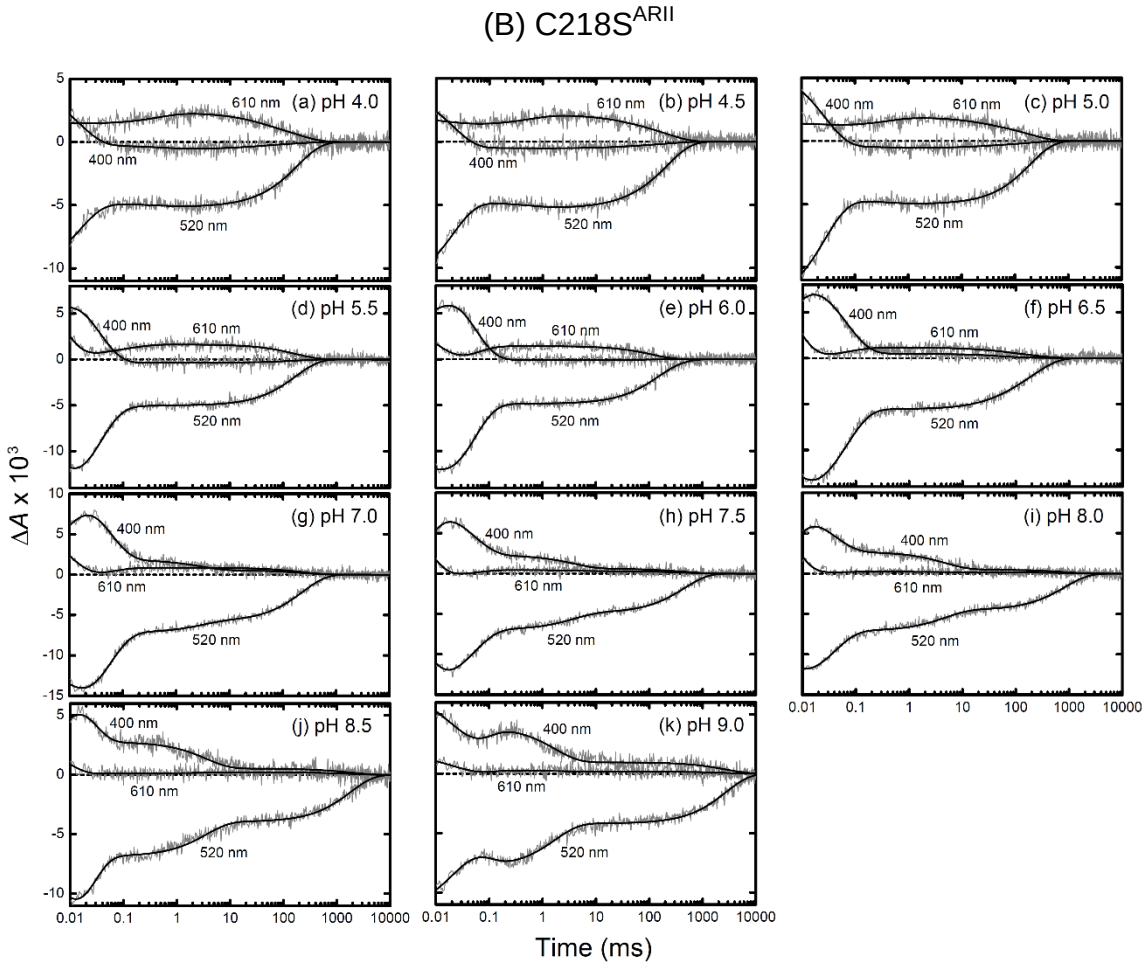

Figure S3: Time-dependent absorbance changes at typical three wavelengths in C218A^{ARII} (A) and C218S^{ARII} (B) at varying pH values.

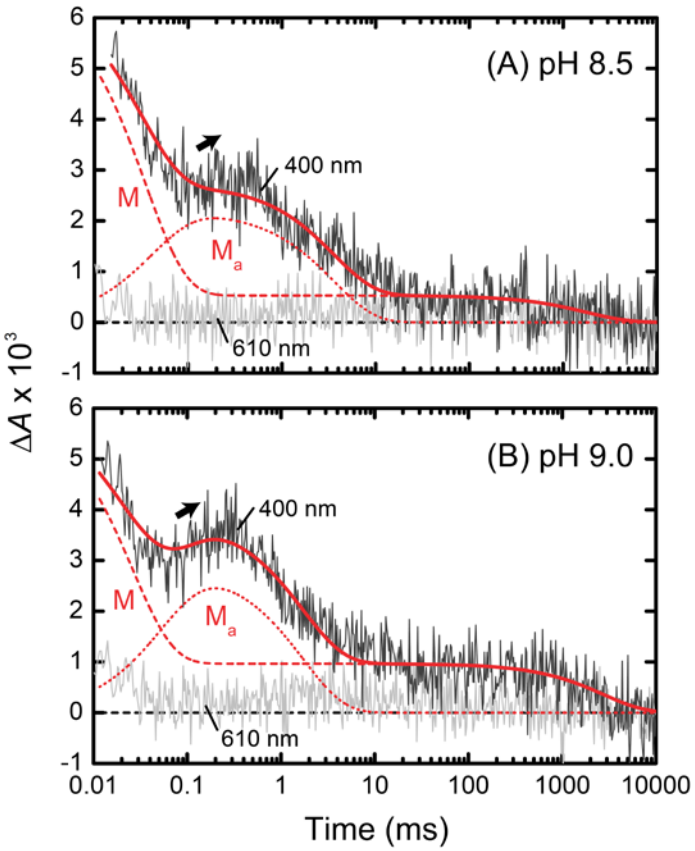

Figure S4: Formation of M_a in C218S^{ARII} under alkaline conditions (pH 8.5 (A) and 9.0 (B)). In two panels, we can observe the increase of the ΔA_{400} signals after their first decay in the early time region prior to ~0.1 ms, which originates from the decay of a normal M. Moreover, these increasing phases appear to agree with the time course of a slower K-decay (monitored at 610 nm) that does not coincide with the rise of normal M. The observation of similar absorption changes was also reported for PR at alkaline pH (≥ ~8.5), which was kinetically explained by assuming the existence of another parallel photocycle during which a M-like photoproduct (M_a) is produced [S3]. Thus, these ΔA_{400} signals were analyzed by a photocycle scheme via two parallel paths like PR, in which M and M_a are independently produced [S3]. Under the assumption that the precursor intermediates of M and M_a do not affect the formation/decay of these two

M-like states due to their sufficiently faster kinetics, the time-dependent fractional concentration changes of M and M_a can be simply represented by the following equations:

$$\Delta M \approx A_1 \exp\left(-t/\tau_1\right) + A_3 \exp\left(-t/\tau_3\right) \quad \text{(Eq. S1)}$$

and

$$\Delta M_a \approx B\frac{\tau_5}{\tau_4 - \tau_5}\left[\exp\left(-t/\tau_4\right) - \exp\left(-t/\tau_5\right)\right] \quad \text{(Eq. S2)}$$

Here, as defined in the text, τ_1 and τ_3 in Eq. S1 are time constants of the first and third decay components of M, whereas A_1 and A_3 are scaling constants for their amplitude. A second decay component (τ_2) cannot be clearly observed, probably due to overlapping with the decay of M_a (τ_5); thus, it was omitted. τ_4, τ_5, and B in Eq. S2 represent time constants of the rise and decay of M_a and a scaling constant for the amplitude of M_a, respectively. A function of the sum of the two equations S1 and S2 noted above ($\Delta A_{400} \approx \Delta M + \Delta M_a$) was used for the fitting. The adequate fitting curves are shown in red continuous lines. Respective calculated fractional changes for M and M_a are shown in red broken and dotted lines, respectively.

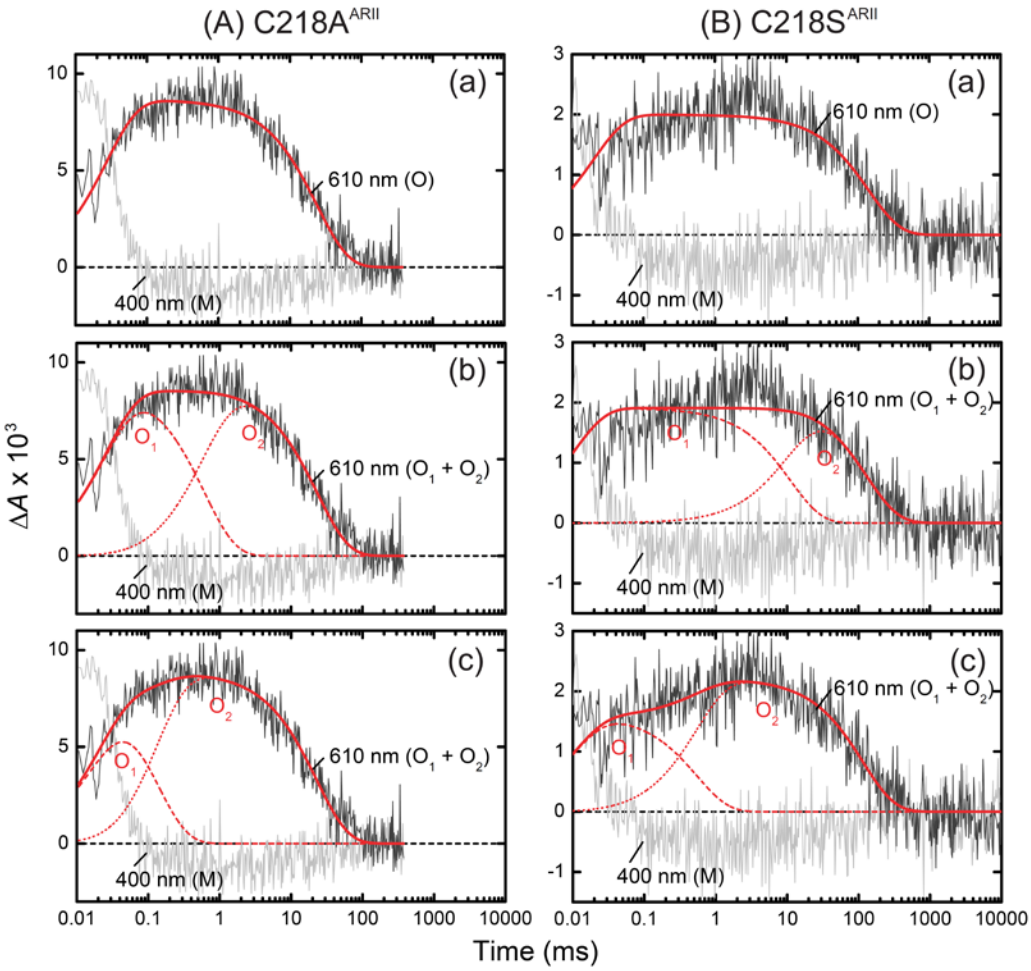

Figure S5: Observation of two O-intermediates in C218A^{ARII} (A) and C218S^{ARII} (B) under acidic condition (pH 4.0). The decreasing phases of the 610 nm-signals originating from K-decay, which is monitored at the early time range (< ~0.1 ms), are not observed at pH 4.0, suggesting sufficiently fast K-decay to be undetectable in our employed apparatus for measurements. As described in the text, the replacement of C218^{ARII} induces the apparent detection of L in the early kinetic photoproducts (P_1 and P_2) (see Fig. 3), which may not contradict the faster K-decay in these mutants. The latter time region of the 610 nm-signal reflects the formation and decay of O. As described previously [S2], the photocycle of the wild-type required the assumption of two sequential Os (O_1 and O_2) with different molar extinction coefficient (ε) values under

lower pH conditions (≤ ~5.5), although O_1 cannot be detected at neutral and basic pH values due to slowing of the N $\rightarrow$ O_1 reaction as the medium pH increases [S1]. The O_2-yield also decreases with further increases in pH. However, in the wild-type, a small amount of O (O_2) was observable even at pH 8.8 [S1]. In contrast, a pH-increase above ~7.5 in $C218^{ARII}$ mutants gave rise to no accumulation of O_2 during their photocycles (Fig. S3). This may be interpretable as the effects of the significantly slower N-decay in these mutants. The kinetic analyses by three models concerning O were performed for the ΔA_{610} signals. The principle of these analyses is described in our previous paper [S2]. The panels (a), (b), and (c) show the fitting results by the models containing single O, two sequential Os (O_1 and O_2) with equal ε, and sequential O_1 and O_2 with different ε values, respectively. The bold continuous red lines represent the best fit curves in respective analyses. The calculated fractional concentration changes of O_1 and O_2 from these analyses are shown in red broken and dotted lines, respectively. Among three analyses, the third scheme (panel (C)) gave the most preferable fitting results for both mutants.

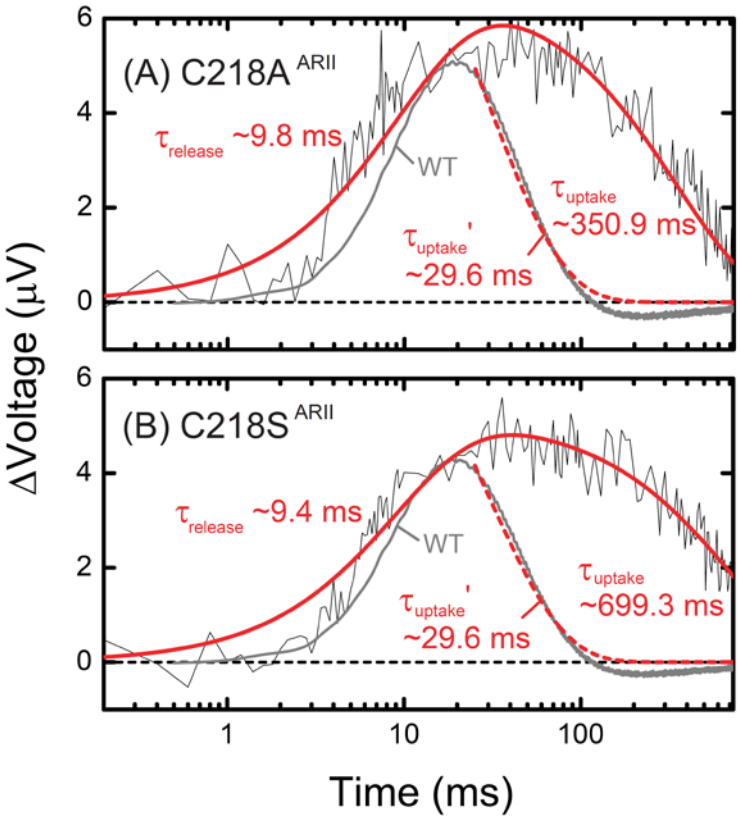

Figure S6: Kinetics of photoinduced proton release and uptake in C218A^{ARII} (A) and C218S^{ARII} (B). The rates of the first proton release and consecutive uptake were estimated by the fitting with the following equation: $\Delta\text{Voltage} \propto \Delta\left[\text{H}^+\right] = C\frac{\tau_{\text{uptake}}}{\tau_{\text{release}} - \tau_{\text{uptake}}}\left[\exp\left(-t/\tau_{\text{release}}\right) - \exp\left(-t/\tau_{\text{uptake}}\right)\right]$, where τ_{release}, τ_{uptake}, and C are the time constants of the first proton release and second uptake, and a constant reflecting the fraction of the subpopulation inducing the initial proton release, respectively [S3]. The continuous red lines in respective panels represent the fit curves. For comparison, the time constant of the H^+-uptake in the wild-type (τ_{uptake}') was also estimated by the fitting for the decreasing phases in the observed signals (continuous

grey lines) with a single exponential equation (broken red lines).

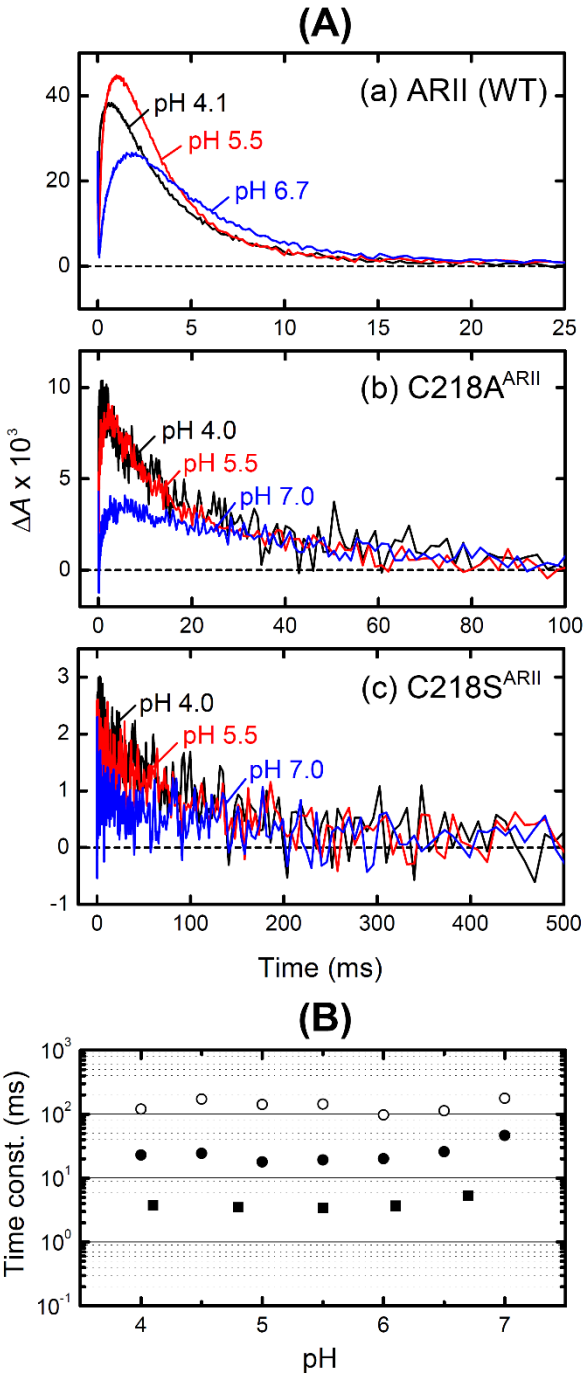

Figure S7: pH dependence of O-decay. (A) Time-dependent absorbance changes at 610 nm in the wild-type (a), C218A^{ARII} (b), and C218S^{ARII} (c) at three pH values. (B) Plot of time constants of O-decay versus pH. The time constants of O-decay in respective proteins (■, wild-type; ●, C218A^{ARII}; ○, C218S^{ARII}) were calculated from the regression

for the decaying phases of the 610 nm-signals with a single exponential equation.

References

[S1] T. Kikukawa, K. Shimono, J. Tamogami, S. Miyauchi, S.Y. Kim, T. Kimura-Someya, M. Shirouzu, K.-H. Jung, S. Yokoyama, N. Kamo, Photochemistry of *Acetabularia* rhodopsin II from a marine plant, *Acetabularia acetabulum*, Biochemistry 50 (2011) 8888-8898.

[S2] J. Tamogami, T. Kikukawa, T. Nara, M. Demura, T. Kimura-Someya, M. Shirouzu, S. Yokoyama, S. Miyauchi, K. Shimono, N. Kamo, Existence of two O-like intermediates in the photocycle of *Acetabularia* rhodopsin II, a light-driven proton pump from a marine alga, Biophys. Physicobiol. 14 (2017) 49-55.

[S3] J. Tamogami, K. Sato, S. Kurokawa, T. Yamada, T. Nara, M. Demura, S. Miyauchi, T. Kikukawa, E. Muneyuki, N. Kamo, Formation of M‒like intermediates in proteorhodopsin in alkali solutions (pH ≥ ~8.5) where the proton release occurs first in contrast to the sequence at lower pH, Biochemistry 55 (2016) 1036-1048.